George Chatzigeorgiou · Nicolas Charalambakis · Fodil Meraghni

A review on the multiscale strategies of dissipative materials under fully coupled thermomechanical conditions

Abstract In this short review, the multiscale modeling of dissipative composites undergoing fully coupled thermomechanical processes is outlined through the models presented in a collection of recent works. The aim is to demonstrate the challenges and limitations of: (1) the multiscale approaches (full-field or mean-field techniques), (2) the computational approaches dealing with complex material systems, (3) the alternative methodologies dedicated to the analysis of composite structures, such as those founded on the data-driven modeling and the model order reduction techniques.

Keywords Multiscale modeling · Dissipative materials · Thermomechanical processes · Data-driven approaches · Model order reduction

1 Introduction

The prediction of the behavior of dissipative composites in regimes under extreme loading conditions is of great technological importance for the aerospace and automotive industry. Novel material systems consisting of complex microstructures have been adopted in lightweight structures with high needs in strength, multi-functionality, and durability. Practical applications require that such structures exhibit long lifetime during cyclic loading conditions. The latter very often trigger dissipative mechanisms related to plastic and viscous phenomena, phase transformation, as well as damage. A key factor in accurately predicting the fatigue behavior of composite media and structures is to identify and capture the energy exchanges during thermomechanical loading cycles [1–3]. In the case of polymer-based composites, for instance, the produced dissipation under repeated loading in inelastic regimes leads to a significant temperature increase, which in turn alters the mechanical response of the structural components [2,4]. Indeed, thermomechanical couplings impact significantly the behavior of semi-crystalline polymer-based composites, especially when the temperature ranges above or below the glass transition temperature. It is thus of vital importance for any multiscale approach dealing with such material systems and structures to incorporate the dissipation at all relevant scales.

Mathematically speaking, dissipativity also provides an a priori stability estimate for the solutions of the system of partial differential equations describing the process, which could possibly exhibit strain discon-

G. Chatzigeorgiou · F. Meraghni (✉)
LEM3 UMR CNRS 7239, Arts et Métiers Institute of Technology, 57070 Metz, France
E-mail: fodil.meraghni@ensam.eu

G. Chatzigeorgiou
E-mail: georges.chatzigeorgiou@ensam.eu

N. Charalambakis
Department of Civil Engineering, Aristotle University of Thessaloniki, 54124 Thessaloniki, Greece
E-mail: charalam@civil.auth.gr

tinuities: Material inhomogeneities may cause inelastic phenomena, such as shear banding or necking. To incorporate the possible discontinuities, mathematical analysis proposed the appropriate functional setting for specific material responses, usually based on the dissipation inequality [5]. On the other hand, the process is smooth over time. The solidness and clarity of the mathematical homogenization theory, as demonstrated through convergence analysis [6–8], the asymptotic expansion method [9,10], and the extension to nonlinear solids [11] permitted the emergence of a variety of computational theories and algorithms. Gamma-convergence theory is a powerful homogenization tool and can be extended to account for complex phenomena, such as bending in metamaterials [12].

Computational homogenization appears to be a reliable method, provided that it is based on the correct functional setting [13–15]. For elastic–plastic with hardening and elastic–viscoplastic materials, the Sobolev space H^1, which is the space with bounded L^2-norm for both the functions and their derivatives, provides, for fixed time, the appropriate functional setting, without safe loading control and with a well-established and popular iterative computational scheme, the return mapping algorithm [15,16]. This is not the case for the elastic–perfectly plastic materials, where strain and dissipation are measures. The process needs a safe loading control. The displacement belongs to the space of bounded variation BD and the process exhibits displacement discontinuities, resulting in strain localization and shear banding, and requires special computational schemes. It is worth noticing that the knowledge of the exact qualitative behavior of solutions of the system of partial differential equations describing the problem (existence, uniqueness, etc. [17]) is needed also for the application of Physics-Informed Neural Networks in order to predict their solution [18].

The overall behavior of viscoelastic, elastoplastic, viscoplastic or damaged composites, or fully coupled thermomechanical models has been studied by several homogenization or micromechanics-based computational methods, such as the higher-order theories [19,20], the theory of thermoviscoelasticity of rubber-like matrix composites [21], the fully implicit formulation of elastoplastic composites [22], the parametric finite volume-based theories [23–26]. Several computational methods have been developed to analyze smart structures with high strength, multifunctionality, and durability. Their thermomechanical behavior under fatigue [4], their magnetomechanical [27,28], and their thermomagnetoelectroelastic response [29] have been studied thoroughly. Micro- to macrotransitions have been also presented for shape memory alloys [30,31] on the basis of a thermomechanical constitutive model [32] using return mapping algorithm. Computational homogenization schemes considering large deformations have also been designed [33]. Second-order homogenization approaches have been also developed for the study of elastoplastic media [34], metamaterials [35]. Their advantage is that they are capable of capturing size effects [36].

For fully coupled thermomechanical processes, the generalized standard material theory [37–39] is often adopted. Many researchers [40–42] assumed different macroscopic responses in order to compose the Gibbs and Helmholtz potentials, as well as the dissipation potential, of this theory and obtain the relation with the microvariables. Fully coupled thermomechanical processes under large deformations have been studied [43] with arbitrary constitutive laws for the components, but the proposed method is based on specific assumptions on the form of the conservation laws in both scales and the correlation between micro- and macrovariables. Moreover, issues concerning the thermodynamic micro- and macroenergy potentials have not been studied. The asymptotic expansion homogenization method (AEHM) to inelastic materials has been applied by many researchers [44,45], without studying the effect of dissipation on the temperature. Models for fully coupled thermomechanical processes have been proposed, but with the very restrictive assumption of an elastic [46] or large deformation elastic [47] or viscoelastic [48] constitutive behavior. The High-Fidelity Generalized Method of Cells has also been adopted in a recent work [49] for thermoelastic–viscoplastic composites. A general model for the fully coupled thermomechanical process that obeys a general constitutive law [50] has been proposed, allowing different inelastic behaviors for the components. The authors presented a homogenization scheme composed by the combination of asymptotic expansion method [9,10] with linearized incremental formulation. More specifically, first the micro- and macroconservation laws are derived, and then, a general energy potential rate is formulated in micro- and macroscale. All macrovariables and macroequations are explicitly defined or computed by a linearized incremental formulation of the homogenization problem. This framework has been fully implemented in FE^2 type of analyses [51]. The main drawback of these type of approaches is the increased computational cost. For this reason, alternative methods have been proposed recently, based on artificial neural networks [52] and model order reduction approaches like the proper generalized decomposition [53].

The organization of the manuscript is as follows: Sects. 2 and 3 introduce the general formalism of the thermomechanical coupled problem for composites and how it is addressed according to the periodic homogenization method. Section 4 presents the general conclusions in terms of equations and variables at the different scales of the composite (microscopic/macroscopic). Section 5 discusses the computational approaches that

can be used for solving the homogenization problem. The analysis of composites under thermomechanical conditions using mean-field methods is the topic of Sect. 6. Section 7 focuses on recent alternative methodologies, such as the artificial neural networks and the model order reduction techniques. The article finishes with a conclusions section.

2 Mathematical homogenization and its limits

Common questions in the multiscale modeling of composite materials concern the definition of the representative volume element (RVE) and the principle of scale separation. Both issues have long been debated in the literature [54–57]. In general, for composites with arbitrary microstructures, considerable ambiguity remains regarding both aspects. In contrast, for periodic composites a rigorous mathematical framework can be established, since the RVE coincides with the periodic unit cell. For this reason, the first part of the present analysis focuses on the well-defined concept of mathematical homogenization in periodic heterogeneous media. For other classes of microstructures, certain assumptions and simplifications are required to ensure that the general results of periodic homogenization remain valid [58].

Let us assume for simplicity that all heterogeneities of a heterogeneous body may be expressed in terms of a small parameter ϵ and that the body $\bar{\mathfrak{B}}$ under consideration is approximated by $\mathfrak{B}^\epsilon$ that exhibits a periodicity ϵ. The body is composed from the repetition of the same unit cell $\mathfrak{B}$. For more general (for instance curvilinear) periodicities, we refer elsewhere [59,60].

In periodic structures, it is assumed [10] that a generic function is of the form

$$\psi^\epsilon(\bar{\boldsymbol{x}}) = \psi\left(\bar{\boldsymbol{x}}, \frac{\bar{\boldsymbol{x}}}{\epsilon}\right) = \psi(\bar{\boldsymbol{x}}, \boldsymbol{x}), \quad \text{periodic with respect to } \boldsymbol{x} = \frac{\bar{\boldsymbol{x}}}{\epsilon}, \tag{2.1}$$

where $\bar{\boldsymbol{x}}$ and $\boldsymbol{x}$ are the macro- and microcoordinates, respectively. In the sequel, every tensor or vector is represented either in indicial notation (for instance x_i) or in a bold character for tensorial notation ($\boldsymbol{x}$). Contrarily to the strongly (i.e., in norm) converging sequences, as the ϵ-independent functions, all oscillating sequences sufficiently regular (for instance, belonging to the space of square-integrable functions) are only weakly convergent sequences.

As an example, let us consider the quasi-static problem of a thermo-visco-elasto-plastic von Mises composite $\mathfrak{B}^\epsilon$ under tractions $t_i^\epsilon(\bar{\boldsymbol{x}}, t)$, body force $b_i^\epsilon(\bar{\boldsymbol{x}}, t)$, radiation $R^\epsilon(\bar{\boldsymbol{x}}, t)$, and heat flux $q_i^\epsilon(\bar{\boldsymbol{x}}, t)$ satisfying the system $\mathcal{P}^\epsilon$: (2.2)-(2.9) supplemented by the free energy potential (2.12) and constrained by the plasticity von Mises conditions (2.13)-(2.15) [58]. The solution of this system is $\left(\sigma_{ij}^\epsilon, u_i^\epsilon, \varepsilon_{ij}^\epsilon, \theta^\epsilon\right)$, where σ_{ij}^ϵ is the stress tensor, u_i^ϵ is the displacement vector, $\varepsilon_{ij}^\epsilon$ is the strain tensor, and θ^ϵ is the temperature, respectively.

$$\frac{\partial \sigma_{ij}^\epsilon}{\partial \bar{x}_j} + \rho^\epsilon b_i^\epsilon = 0 \text{ in } \mathcal{B}^\epsilon, \ i = 1, 2, 3, \tag{2.2}$$

$$\frac{\partial q_i^\epsilon}{\partial \bar{x}_i} - r^\epsilon - \rho^\epsilon R^\epsilon = 0 \text{ in } \mathcal{B}^\epsilon, \ i = 1, 2, 3, \tag{2.3}$$

$$\varepsilon_{ij}^\epsilon = \frac{1}{2}\left(\frac{\partial u_i^\epsilon}{\partial \bar{x}_j} + \frac{\partial u_j^\epsilon}{\partial \bar{x}_i}\right) \text{ in } \mathcal{B}^\epsilon, \ i, j = 1, 2, 3, \tag{2.4}$$

$$q_i^\epsilon = k_{ij}^\epsilon \nabla_j \theta \text{ in } \mathcal{B}^\epsilon, \ i = 1, 2, 3, \tag{2.5}$$

$$\sigma_{ij}^\epsilon n_j^\epsilon = t_i^*, \ i = 1, 2, 3, \text{ on } \partial\mathcal{B}_t^\epsilon, \tag{2.6}$$

$$q_i^\epsilon n_i^\epsilon = q^*, \ i = 1, 2, 3, \text{ on } \partial\mathcal{B}_Q^\epsilon, \tag{2.7}$$

$$u_i^\epsilon = u_i^*, \ i = 1, 2, 3, \text{ on } \partial\mathcal{B}_c^\epsilon, \tag{2.8}$$

$$\theta^\epsilon = \theta^* \text{ in } \partial\mathcal{B}_T^\epsilon, \tag{2.9}$$

In the above expressions, ρ^ϵ is the density, the energy function r^ϵ is given in terms of internal energy $\mathcal{E}^\epsilon$ [39,58] by

$$r^\epsilon = \sigma_{ij}^\epsilon \dot{\varepsilon}_{ij}^\epsilon - \dot{\mathcal{E}}^\epsilon, \tag{2.10}$$

$$\mathcal{E}^\epsilon = \Psi^\epsilon + \theta^\epsilon \eta^\epsilon, \tag{2.11}$$

while Ψ^ϵ, η^ϵ are the Helmholtz potential and the specific entropy, respectively, where [50]

$$\begin{aligned}
&\Psi^\epsilon(\varepsilon^\epsilon_{mn}, \theta^\epsilon, \varepsilon^{p\epsilon}_{mn}, p^\epsilon) \\
&= \frac{1}{2}[\varepsilon^\epsilon_{ij} - \varepsilon^{p\epsilon}_{ij} - \alpha^\epsilon(\theta^\epsilon - \theta^\epsilon_0)]C^\epsilon_{ijkl}[\varepsilon^\epsilon_{kl} - \varepsilon^{p\epsilon}_{kl} - \alpha^\epsilon(\theta^\epsilon - \theta^\epsilon_0)] \\
&+c^\epsilon_0\left[(\theta^\epsilon - \theta^\epsilon_0) - \theta^\epsilon \ln\left(\frac{\theta^\epsilon}{\theta^\epsilon_0}\right)\right] - \eta^\epsilon_0\theta^\epsilon + E^\epsilon_0 + F^\epsilon(p^\epsilon),
\end{aligned} \tag{2.12}$$

and the yield surface Φ^ϵ is expressed as [50,58]

$$\Phi^\epsilon = \bar{\sigma}^\epsilon - \frac{\partial F^\epsilon}{\partial p^\epsilon} - \sigma^\epsilon_Y - K^\epsilon_a(\dot{p}^\epsilon)^{\frac{1}{N^\epsilon_a}}. \tag{2.13}$$

Moreover,

$$\dot{\varepsilon}^{p\epsilon}_{ij} = \dot{p}^\epsilon \Lambda^\epsilon_{ij} = \dot{p}^\epsilon \frac{\partial \Phi^\epsilon}{\partial \sigma^\epsilon_{ij}} = \dot{p}^\epsilon \frac{3s^\epsilon_{ij}}{2\bar{\sigma}^\epsilon}, \tag{2.14}$$

$$\Phi^\epsilon \le 0, \quad \dot{p}^\epsilon \ge 0, \quad \Phi^\epsilon \dot{p}^\epsilon = 0, \tag{2.15}$$

$$\sigma^\epsilon_{ij} = C^\epsilon_{ijkl}[\varepsilon^\epsilon_{kl} - \varepsilon^{p\epsilon}_{kl} - \alpha^\epsilon_{kl}(\theta^\epsilon - \theta^\epsilon_0)], \tag{2.16}$$

where α^ϵ_{kl} is the thermal expansion coefficient tensor and s^ϵ_{ij} denotes the deviatoric part of the stress. It is noted that the constitutive law (2.16) produced from the free energy (2.12) and the plasticity potential (2.13) satisfies the Clausius–Duhem inequality. Mathematical homogenization consists in passing to the limit for $\epsilon \to 0$ in $\mathcal{P}^\epsilon$ and looking for the "homogenized" problem, coefficients (called effective coefficients if the homogenized material is homogeneous) and solution [6,7]. However, in general, passing to the limit by using only nonlinear analysis techniques is not easy since energy equation, constitutive equation and, possibly, more general boundary conditions are nonlinear expressions of oscillating functions. There are some very few exceptions in one dimensional problems, where the above techniques are efficient [61].

In general, non-linearities put serious difficulties of applying a full mathematical homogenization. We simply note only what one can easily do: In view of (2.2), the equation of equilibrium after multiplication by a test function $\varphi^\epsilon_i(\bar{\boldsymbol{x}})$, integration over $\mathfrak{B}^\epsilon$, using the divergence theorem and (2.6), (2.8), with, for simplicity, $u^*_i = 0$, gives

$$\int_{\mathfrak{B}^\epsilon} \sigma^\epsilon_{ij}\frac{\partial \varphi^\epsilon_i}{\partial \bar{x}_j} d\bar{\boldsymbol{x}} = \int_{\mathfrak{B}^\epsilon} \rho^\epsilon b^\epsilon_i \varphi^\epsilon_i d\bar{\boldsymbol{x}} + \int_{S^\epsilon_t} t^*_i \varphi^\epsilon_i dS \quad \forall \varphi^\epsilon_i \text{ in } L^2(\mathfrak{B}^\epsilon), \tag{2.17}$$

Similarly, from (2.3), (2.7), (2.9) with $\theta^*_i = 0$,

$$\int_{\mathfrak{B}^\epsilon} q^\epsilon_i \frac{\partial \varphi^\epsilon}{\partial \bar{x}_i} d\bar{\boldsymbol{x}} = \int_{\mathfrak{B}^\epsilon} (r^\epsilon + \rho^\epsilon \mathcal{R}^\epsilon_i)\varphi^\epsilon d\bar{\boldsymbol{x}} + \int_{S^\epsilon_Q} q^* \varphi^\epsilon dS \quad \forall \varphi^\epsilon \text{ in } L^2(\mathfrak{B}^\epsilon). \tag{2.18}$$

Under sufficient regularity assumptions on data, it is known that, for fixed ϵ, there exists a unique solution and that, for fixed time, all unknown functions belong at least to $L^2(\mathfrak{B}^\epsilon)$. Then we can pass to the limit in (2.17) for $\epsilon \to 0$. Assuming that $\varphi^\epsilon_i \equiv \varphi_i$, and using the weak convergence limit yield

$$\int_{\bar{\mathcal{B}}} \frac{1}{|\mathcal{B}|}\left(\int_{\mathcal{B}} \sigma^0_{ij} d\bar{\boldsymbol{x}}\right)\frac{\partial \varphi_i}{\partial \bar{x}_j} d\bar{\boldsymbol{x}} = \int_{\bar{\mathcal{B}}} \langle \rho^\epsilon b^\epsilon_i \rangle \varphi_i d\bar{\boldsymbol{x}} + \int_{\partial \bar{\mathcal{B}}_t} \bar{t}_i \varphi_i dS \; \forall \varphi_i \text{ in } L^2(\bar{\mathcal{B}}), \tag{2.19}$$

from which it is obtained that the mean stress over the unit cell,

$$\bar{\sigma}_{ij}(\bar{\boldsymbol{x}}) = \frac{1}{|\mathcal{B}|}\int_{\mathcal{B}} \sigma^0_{ij}(\bar{\boldsymbol{x}}, \boldsymbol{x}) \mathrm{d}\boldsymbol{x}, \tag{2.20}$$

satisfies the homogenized equation of equilibrium (2.19) for the weak limits of the traction and body forces.

3 Asymptotic expansion homogenization and its limits

In order to pass to the limit in (2.17) and (2.18), an additional type of convergence using oscillating test functions $\varphi^\epsilon(\boldsymbol{x})$ is required, namely the two-scale convergence [62,63]. An important example of two-scale converging functions is given by the functions having an asymptotic expansion of the form

$$\psi^\epsilon(\bar{\boldsymbol{x}}) = \psi\left(\bar{\boldsymbol{x}}, \frac{\bar{\boldsymbol{x}}}{\epsilon}\right) = \psi^0\left(\bar{\boldsymbol{x}}, \frac{\bar{\boldsymbol{x}}}{\epsilon}\right) + \epsilon\psi^1\left(\bar{\boldsymbol{x}}, \frac{\bar{\boldsymbol{x}}}{\epsilon}\right) + \epsilon^2\psi^2\left(\bar{\boldsymbol{x}}, \frac{\bar{\boldsymbol{x}}}{\epsilon}\right) + ..., \tag{3.1}$$

where all functions are periodic in $\boldsymbol{x} = \dfrac{\bar{\boldsymbol{x}}}{\epsilon}$. Hence, it is natural to assume that all functions of the heterogeneous problem are of the form (3.1). Note that the two-scale limit ψ^0 carries more information than the weak limit

$$\langle\psi(\boldsymbol{x})\rangle = \frac{1}{|\mathfrak{B}|}\int_{\mathfrak{B}} \psi^0(\boldsymbol{x}, \boldsymbol{x})\mathrm{d}\boldsymbol{x}.$$

A lemma of particular interest is the two-scale convergence of derivatives of H^1-functions [62,63], i.e., square-integrable functions having square-integrable first derivatives. Application of this lemma to the displacement gradient yields to the following assertion, revealing the existence of the gradient of the displacement fluctuation $\boldsymbol{u}^1$: If the displacement $\boldsymbol{u}^\epsilon(\bar{\boldsymbol{x}})$ converges weakly in $H^1(\bar{\mathcal{B}})$ to $\boldsymbol{u}(\bar{\boldsymbol{x}})$, then $\boldsymbol{u}^\epsilon(\bar{\boldsymbol{x}})$ two-scale converges to $\boldsymbol{u}^0 \equiv \boldsymbol{u}(\bar{\boldsymbol{x}})$ and there exists a microdisplacement $\boldsymbol{u}^1$ such that

$$\begin{aligned}&\lim_{\epsilon\to 0}\int_{\bar{\mathcal{B}}} \boldsymbol{\varepsilon}^\epsilon(\bar{\boldsymbol{x}}) : \boldsymbol{\varphi}^\epsilon(\bar{\boldsymbol{x}})d\bar{\boldsymbol{x}}\\ &\quad= \int_{\bar{\mathcal{B}}}\frac{1}{|\mathcal{B}|}\int_{\mathcal{B}}\left[\bar{\boldsymbol{\varepsilon}}(\bar{\boldsymbol{x}}) + \mathrm{sym}\frac{\partial \boldsymbol{u}^1(\bar{\boldsymbol{x}}, \boldsymbol{x})}{\partial \boldsymbol{x}}\right] : \boldsymbol{\varphi}(\bar{\boldsymbol{x}}, \boldsymbol{x})\mathrm{d}\boldsymbol{x}d\bar{\boldsymbol{x}},\end{aligned} \tag{3.2}$$

for every $\boldsymbol{\varphi}(\bar{\boldsymbol{x}}, \boldsymbol{x}) \in L^2(\bar{\mathfrak{B}} \times \mathfrak{B})$. The fact that the displacement two scale converges to the first term of its asymptotic expansion $\boldsymbol{u}^0$ which is independent of the microcoordinate is formally proven by taking the gradient of the expanded form (3.1) of the displacement and considering the coefficient of ϵ^{-1} equal to zero in order to exclude infinite strains. Therefore, the first term of the strain coincides with the macrostrain $\bar{\varepsilon}_{ij} = \dfrac{1}{2}\left(\dfrac{\partial u_i^0}{\partial \bar{x}_j} + \dfrac{\partial u_i^0}{\partial \bar{x}_j}\right)$. Regarding the temperature, one can verify the existence of both a microtemperature independent of the microcoordinate $\theta^0(\bar{x}) = \bar{\theta}(\bar{x})$ and a temperature fluctuation gradient, $\nabla_x\boldsymbol{\theta}^1(\bar{\boldsymbol{x}}, \boldsymbol{x})$. Now it is possible to pass to the limit in (2.17) with $\varphi_i^\epsilon = u_i^\epsilon$ and using that $\bar{\boldsymbol{\varepsilon}}$ is independent of $\boldsymbol{x}$ and that $\bar{\boldsymbol{\sigma}} = \dfrac{1}{|\mathfrak{B}|}\displaystyle\int_{\mathfrak{B}} \boldsymbol{\sigma}^0\mathrm{d}\boldsymbol{x}$, the following equations are obtained:

$$\int_{\bar{\mathcal{B}}} \bar{\boldsymbol{\sigma}} : \nabla\boldsymbol{u}d\bar{\boldsymbol{x}} = \int_{\bar{\mathcal{B}}}\langle\rho^\epsilon\boldsymbol{b}^\epsilon\rangle\cdot\boldsymbol{u}d\bar{\boldsymbol{x}} + \int_{\bar{\mathcal{B}}_t}\bar{\boldsymbol{t}}\cdot\boldsymbol{u}dS \;\; \forall\, u_i \in L^2(\bar{\mathfrak{B}} \times \mathfrak{B}), \tag{3.3}$$

$$\int_B \mathrm{div}_x\boldsymbol{\sigma}^0\cdot\boldsymbol{v}\mathrm{d}\boldsymbol{x} = 0, \;\; \forall\, v_i \in L^2(\bar{\mathfrak{B}} \times \mathfrak{B}). \tag{3.4}$$

Equation (3.3) is the macroequilibrium equation and (3.4) is the cell problem. The microstress $\boldsymbol{\sigma}^0$ is the first term of the expansion (3.1). Similarly, passing to the limit in (2.18),

$$-\int_{\bar{\mathfrak{B}}}\bar{\boldsymbol{q}}\cdot\nabla\boldsymbol{\varphi}d\bar{\boldsymbol{x}} = \int_{\mathfrak{B}}(\bar{r} + \langle\rho^\epsilon\mathcal{R}^\epsilon\rangle)\varphi d\bar{\boldsymbol{x}} + \int_{S_Q} q^*\varphi dS, \quad \forall\varphi \in L^2(\bar{\mathfrak{B}} \times \mathfrak{B}), \tag{3.5}$$

$$\int_B \mathrm{div}_x\boldsymbol{q}^0 v\mathrm{d}\boldsymbol{x} = 0, \;\; \forall\, v \in L^2(\bar{\mathfrak{B}} \times \mathfrak{B}). \tag{3.6}$$

The convergence results presented above are independent of the constitutive law of the materials.

It is obvious that one cannot easily continue in this way in all remaining equations of the system $\mathcal{P}^\epsilon$: (2.2)-(2.9) supplemented by the free energy potential (2.12) and constrained by the plasticity von Mises conditions (2.13)-(2.15). Additionally, the limitation to a specific constitutive framework as in the above example is very restrictive. A complete asymptotic expansion homogenization method for the fully coupled thermomechanical

Table 1 Variables and conservation laws in both scales

Variable/equation	Microscale	Macroscale
Displacement	$\boldsymbol{u} = \bar{\boldsymbol{u}}$	$\bar{\boldsymbol{u}}$
Strain	$\boldsymbol{\varepsilon} = \bar{\boldsymbol{\varepsilon}} + \text{grad}_{\text{sym}}\tilde{\boldsymbol{u}}$	$\bar{\boldsymbol{\varepsilon}} = \overline{\text{grad}}_{\text{sym}}\bar{\boldsymbol{u}} = \langle\boldsymbol{\varepsilon}\rangle$
Stress	$\boldsymbol{\sigma}$	$\bar{\boldsymbol{\sigma}} = \langle\boldsymbol{\sigma}\rangle$
Density	ρ	$\bar{\rho} = \langle\rho\rangle$
Body forces	$\boldsymbol{b}$	$\bar{\boldsymbol{b}} = \langle\rho\boldsymbol{b}\rangle/\bar{\rho}$
Internal energy	$\mathcal{E}$	$\bar{\mathcal{E}} = \langle\mathcal{E}\rangle$
Energy rate term r	$r = \boldsymbol{\sigma} : \dot{\boldsymbol{\varepsilon}} - \dot{\mathcal{E}}$	$\bar{r} = \bar{\boldsymbol{\sigma}} : \dot{\bar{\boldsymbol{\varepsilon}}} - \dot{\bar{\mathcal{E}}} = \langle r\rangle$
Heat flux	$\boldsymbol{q}$	$\bar{\boldsymbol{q}} = \langle\boldsymbol{q}\rangle$
Heat sources	$\mathcal{R}$	$\bar{\mathcal{R}} = \langle\rho\mathcal{R}\rangle/\bar{\rho}$
Temperature	$\theta = \bar{\theta}$	$\bar{\theta}$
Temperature gradient	$\boldsymbol{\nabla\theta} = \overline{\boldsymbol{\nabla\theta}} + \text{grad}\,\tilde{\theta}$	$\overline{\boldsymbol{\nabla\theta}} = \overline{\text{grad}}\bar{\theta} = \langle\boldsymbol{\nabla\theta}\rangle$
Specific entropy	η	$\bar{\eta} = \langle\eta\rangle$
Equilibrium	$\text{div}\,\boldsymbol{\sigma} = \boldsymbol{0}$	$\bar{\rho}\bar{\boldsymbol{b}} + \overline{\text{div}}\,\bar{\boldsymbol{\sigma}} = \boldsymbol{0}$
Angular momentum	$\boldsymbol{\sigma} = \boldsymbol{\sigma}^T$	$\bar{\boldsymbol{\sigma}} = \bar{\boldsymbol{\sigma}}^T$
Energy balance	$\text{div}\,\boldsymbol{q} = 0$	$\bar{r} - \overline{\text{div}}\,\bar{\boldsymbol{q}} + \bar{\rho}\bar{\mathcal{R}} = 0$
Entropy inequality	$\bar{\theta}\dot{\eta} + r - \frac{\boldsymbol{q}}{\theta}\cdot\boldsymbol{\nabla\theta} \geq 0$	$\bar{\theta}\dot{\bar{\eta}} + \bar{r} - \frac{\bar{\boldsymbol{q}}}{\bar{\theta}}\cdot\overline{\boldsymbol{\nabla\theta}} \geq 0$

problem under a general constitutive law [50] has been applied to define all variables and all equations in both scales. This allowed the complete description of the interplay between micro- and macroscale by the derivation of the micro- and the macroconservation laws and by the formulation of a general energy potential in both scales. Therefore, equation of equilibrium (3.3), energy equation (3.5), and the two sets of cell problems (3.4) and (3.6) can be used for inelastic problems by combining the global finite element formulation of (3.3), (3.5), with a Newton–Raphson iterative solution based on a constitutive law algorithm that uses the concept of tangent modulus [50,58]. A flavor of this method is given later in this manuscript.

It should be pointed out that the asymptotic expansion homogenization allows to identify higher-order terms, which are important in cases where ϵ is not sufficiently small [64,65]. While, from a mathematical point of view, higher-order homogenization strategies render consistent results, from a thermodynamic perspective, several questions are raised. When higher terms of ϵ are taken into account, the microscopic stress $\boldsymbol{\sigma}^{(0)}$ becomes a function of the macroscopic temperature gradient. Consequently, its volume average (i.e., the macroscopic stress) is also a direct function of the macroscopic temperature gradient. The latter violates classical thermodynamic arguments for a generalized standard material at the macroscopic scale. Thus, in this case, the homogenized response does not represent a standard material. Another issue arises in connection with the second law of thermodynamics (last line of Table 1). At the macroscale, higher-order terms lead to nonuniformity of the microtemperature and prevent a clean separation between (i) the product of temperature and the entropy rate, and (ii) the product of the temperature gradient and the heat flux. As a result, the definition of macroscopic entropy becomes ambiguous, and a Fourier-type macroscopic law does not emerge naturally [50].

4 Formal periodic homogenization of functions and equations

By assuming the asymptotic series expansion (3.1) for all functions entering equations of the problem and taking formally $\epsilon \to 0$ [9,10], one can find the homogenized expressions shown in Table 1 that summarizes the various variables and equations at both the micro- and macroscale [50,58]. In this table, the superscript (0) of the first asymptotic expansion terms is omitted and the superscript (1) of the displacement fluctuation gradient and the temperature fluctuation gradient is substituted with a tilde above the variable.

Furthermore, by assuming the same form of asymptotic expansion for the various thermodynamic quantities (thermodynamic potential, internal variables, dissipation, etc.), Tables 2 and 3 are produced, showing both micro- and macroscale expressions.

One important outcome of the zeroth order asymptotic expansion is that, at the microscopic scale, the temperature is uniform and equal to the macroscopic temperature, whereas the microscopic temperature gradient varies within the RVE. Let us see how the energy conservation is obtained. The internal energy rate is written

Table 2 Microscale expressions related with the constitutive law

Expression	Microscale
Helmholtz free energy	$\Psi = \mathcal{E} - \eta\bar{\theta} := \Psi(\boldsymbol{\varepsilon}, \bar{\theta}, \boldsymbol{\xi})$
Gibbs free energy	$G = \mathcal{E} - \eta\bar{\theta} - \boldsymbol{\sigma} : \boldsymbol{\varepsilon} := G(\boldsymbol{\sigma}, \bar{\theta}, \boldsymbol{\xi})$
Intrinsic dissipation	$\gamma_{\text{loc}} = -\frac{\partial \Psi}{\partial \boldsymbol{\xi}} : \dot{\boldsymbol{\xi}}$ or $\gamma_{\text{loc}} = -\frac{\partial G}{\partial \boldsymbol{\xi}} : \dot{\boldsymbol{\xi}}$
Rate of Helmholtz free energy	$\dot{\Psi} = \boldsymbol{\sigma} : \dot{\boldsymbol{\varepsilon}} - \eta\dot{\bar{\theta}} + \frac{\partial \Psi}{\partial \boldsymbol{\xi}} : \dot{\boldsymbol{\xi}}$
Rate of Gibbs free energy	$\dot{G} = -\boldsymbol{\varepsilon} : \dot{\boldsymbol{\sigma}} - \eta\dot{\bar{\theta}} + \frac{\partial G}{\partial \boldsymbol{\xi}} : \dot{\boldsymbol{\xi}}$

Table 3 Macroscale expressions related with the constitutive law

Expression	Macroscale
Helmholtz free energy	$\bar{\Psi} = \langle \Psi \rangle = \bar{\mathcal{E}} - \bar{\eta}\bar{\theta}$
Gibbs free energy	$\bar{G} = \langle G \rangle = \bar{\mathcal{E}} - \bar{\eta}\bar{\theta} - \bar{\boldsymbol{\sigma}} : \bar{\boldsymbol{\varepsilon}}$
Intrinsic dissipation	$\bar{\gamma}_{\text{loc}} = \langle \gamma_{\text{loc}} \rangle$
Rate of Helmholtz free energy	$\dot{\bar{\Psi}} = \bar{\boldsymbol{\sigma}} : \dot{\bar{\boldsymbol{\varepsilon}}} - \bar{\eta}\dot{\bar{\theta}} - \bar{\gamma}_{\text{loc}}$
Rate of Gibbs free energy	$\dot{\bar{G}} = -\bar{\boldsymbol{\varepsilon}} : \dot{\bar{\boldsymbol{\sigma}}} - \bar{\eta}\dot{\bar{\theta}} - \bar{\gamma}_{\text{loc}}$

in terms of heat sources per unit mass $\mathcal{R}^\epsilon$ as

$$\dot{\mathcal{E}}^\epsilon = \boldsymbol{\sigma}^\epsilon : \dot{\boldsymbol{\varepsilon}}^\epsilon - \text{div}\boldsymbol{q}^\epsilon + \rho^\epsilon \mathcal{R}^\epsilon \tag{4.1}$$

or

$$r^\epsilon - \text{div}\boldsymbol{q}^\epsilon + \rho^\epsilon \mathcal{R}^\epsilon = 0. \tag{4.2}$$

Replacing in (4.1) both sides with the asymptotic expansions of all functions yields

$$\dot{\mathcal{E}}^{(0)} + \epsilon ... = \boldsymbol{\sigma}^{(0)} : \dot{\boldsymbol{\varepsilon}}^{(0)} - \overline{\text{div}}\boldsymbol{q}^{(0)} - \text{div}\boldsymbol{q}^{(1)} + \rho^{(0)}\mathcal{R}^{(0)} - \frac{1}{\epsilon}\text{div}\boldsymbol{q}^{(0)} + \epsilon ... \tag{4.3}$$

in which the term with coefficient ϵ^{-1} should vanish giving the microequation of energy [46,47]

$$\text{div}\boldsymbol{q}^{(0)} = 0. \tag{4.4}$$

The macroequation of energy is obtained by averaging $\dot{\mathcal{E}}^{(0)}$ over the unit cell. On the right side, since $\boldsymbol{q}^{(1)}$ is periodic, $\langle \text{div}\boldsymbol{q}^{(1)} \rangle = 0$ [48] and using Hill–Mandel lemma,

$$\dot{\bar{\mathcal{E}}} = \bar{\boldsymbol{\sigma}} : \dot{\bar{\boldsymbol{\varepsilon}}} - \overline{\text{div}}\bar{\boldsymbol{q}} + \bar{\rho}\bar{R}, \tag{4.5}$$

where $\bar{\mathcal{R}} = \dfrac{\langle \rho^{(0)}\mathcal{R}^{(0)} \rangle}{\bar{\rho}}$. Moreover,

$$r^{(0)} - \text{div}\boldsymbol{q}^{(0)} + \rho^{(0)}\mathcal{R}^{(0)} = 0.$$

It is concluded that, regarding all variables and energy equation, the process is stable under homogenization. On the contrary, the constitutive equations need a special attention. Since internal energy, Helmholtz and Gibbs potentials are supposed to depend, respectively, as follows

$$\mathcal{E}^\epsilon = \mathcal{E}^\epsilon(\boldsymbol{\varepsilon}^\epsilon, \eta^\epsilon, \boldsymbol{\xi}^\epsilon), \quad \Psi^\epsilon = \Psi^\epsilon(\boldsymbol{\varepsilon}^\epsilon, \theta^\epsilon, \boldsymbol{\xi}^\epsilon), \quad \mathcal{G}^\epsilon = \mathcal{G}^\epsilon(\boldsymbol{\sigma}^\epsilon, \theta^\epsilon, \boldsymbol{\xi}^\epsilon), \tag{4.6}$$

taking differentials of Ψ^ϵ and $\mathcal{G}^\epsilon$ and using the postulates

$$\boldsymbol{\sigma}^\epsilon = \frac{\partial \mathcal{E}^\epsilon}{\partial \boldsymbol{\varepsilon}^\epsilon}, \quad \theta^\epsilon = \frac{\partial \mathcal{E}^\epsilon}{\partial \eta^\epsilon},$$

as well as (2.11), one obtains

$$\dot{\Psi}^{(\epsilon)} = \frac{\partial \Psi^\epsilon}{\partial \boldsymbol{\varepsilon}^\epsilon} : \dot{\boldsymbol{\varepsilon}}^\epsilon + \frac{\partial \Psi^\epsilon}{\partial \theta^\epsilon}\dot{\theta}^\epsilon + \frac{\partial \Psi^\epsilon}{\partial \boldsymbol{\xi}^\epsilon} : \dot{\boldsymbol{\xi}}^\epsilon = \boldsymbol{\sigma} : \dot{\boldsymbol{\varepsilon}}^\epsilon - \eta^\epsilon\dot{\theta}^\epsilon - \gamma^\epsilon_{\text{loc}}, \tag{4.7}$$

where $\gamma^{\epsilon}_{\text{loc}}$ is the intrinsic dissipation defined by

$$\gamma^{\epsilon}_{\text{loc}} = -\frac{\partial \Psi^{\epsilon}}{\partial \boldsymbol{\xi}^{\epsilon}} : \dot{\boldsymbol{\xi}}^{\epsilon}. \tag{4.8}$$

All functions, including $\frac{\partial \Psi^{\epsilon}}{\partial \boldsymbol{\xi}^{\boldsymbol{\epsilon}}} : \dot{\boldsymbol{\xi}}^{\epsilon}$, are expanded and give the microequations of potentials

$$\begin{aligned} \Psi^{(0)} &= \mathcal{E}^{(0)} - \eta^{(0)}\bar{\theta}, \\ \dot{\Psi}^{(0)} &= \boldsymbol{\sigma}^{(0)} : \dot{\boldsymbol{\varepsilon}}^{(0)} - \eta^{(0)}\dot{\bar{\theta}} - \gamma^{(0)}_{\text{loc}}. \end{aligned} \tag{4.9}$$

Since $\Psi^{(0)} = \Psi^{(0)}(\boldsymbol{\varepsilon}^{(0)}, \bar{\theta}, \boldsymbol{\xi}^{(0)})$, the microstress $\boldsymbol{\sigma}^{(0)} = \frac{\partial \Psi^{(0)}}{\partial \boldsymbol{\varepsilon}^{(0)}}$ depends on the macrotemperature. Averaging and using Hill–Mandel lemma,

$$\begin{aligned} \bar{\Psi} &= \bar{\mathcal{E}} - \bar{\eta}\bar{\theta}, \\ \dot{\Psi} &= \bar{\boldsymbol{\sigma}} : \dot{\bar{\boldsymbol{\varepsilon}}} - \bar{\eta}\dot{\bar{\theta}} - \bar{\gamma}_{\text{loc}}. \end{aligned} \tag{4.10}$$

The homogenized intrinsic dissipation $\bar{\gamma}_{\text{loc}} = \langle \gamma_{\text{loc}} \rangle$ cannot be expressed in terms of macroscopic functions only, as the rest of functions included in the potential rate, but depends on the complete set of internals variables. Products of oscillating functions appear after time differentiation of functions depending on internal variables, prohibiting analytical homogenized energy and dissipation [66]. In mechanical terms, this is due to the fact that plastic strain does not converge to a limit [11]. Thus, the energy equation cannot be put in analytical form. One way to bypass this issue is by considering a simplified expression with a properly chosen finite set of internal state variables [67].

We close this Section by an important remark [11]: From (3.2), we can express the displacement in local coordinates in terms of the macrostrain and the fluctuating periodic term $\tilde{u}_i \equiv u^{!}_i$ as follows

$$u_i = \bar{\varepsilon}_{ij} x_j + \tilde{u}_i. \tag{4.11}$$

Equivalently for the temperature

$$\theta = \overline{\nabla\theta}_i x_i + \tilde{\theta}. \tag{4.12}$$

It is worth noticing that (4.12) is utilized only for the microscopic energy balance equation. For the microscopic equilibrium, the temperature is considered constant, equal to the macroscopic one. This is consistent with the zeroth-order asymptotic homogenization theory [46–48].

5 Computational approaches for periodic homogenization

As it was noticed, the constitutive law is complicated and internal variables enter implicit expressions, demanding a first linearization in time and a second linearization of the nonlinear equations.

When dealing with pure mechanical response and complex nonlinear behavior, full-field computational homogenization schemes have been developed extensively for the study of composites. The finite element (FE)-based periodic homogenization framework has been employed to analyze various constitutive responses for composites, like elastoplastic [22,68], viscoelastic, viscoplastic, damageable and combined [69–71], or phase transformation mechanisms in shape memory alloy composites [72]. Viscoplasticity coupled with damage for composites has been analyzed through the combination of FE and Voronoi cells [73]. A popular numerical implementation of the periodic homogenization theory is the Fast Fourier Transforms (FFT) [74]. This technique has been employed in many recent studies [75–77], providing a computationally more efficient strategy than the FE computations. Another methodology discussed in the literature considers the method of cells [78]. The finite volume homogenization approach has also been developed for the study of elastoplastic [24], viscoelastic [79,80], and damage [81] response of composites. The periodic homogenization framework can be also adjusted to account for cylindrically orthotropic behavior of the fibers [82], a special case of which are the fuzzt fibers [83].

Concerning fully coupled thermomechanical processes, several authors [43,50,58,84] have proposed a numerical scheme based on the well-known return mapping algorithm. In brief, macroscale and cell problem are solved simultaneously by an iterative scheme (Fig. 1 and Tables 4, 5, 6).

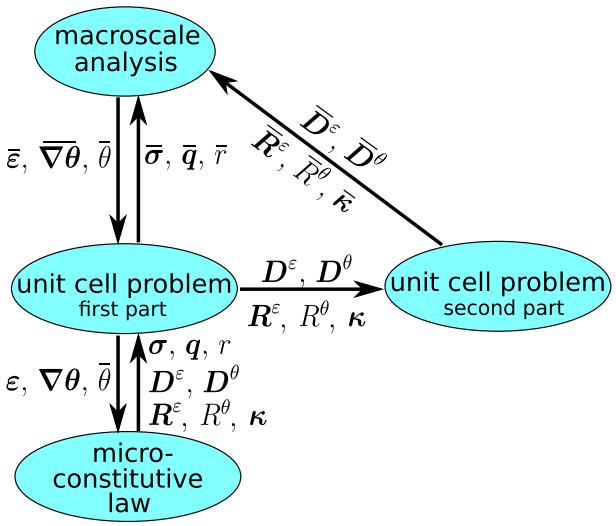

Fig. 1 Detailed homogenization scheme based on the return mapping algorithm [58]

Table 4 Algorithm for the first part of the unit cell problem [58]

1. At time step n, everything is known in both scales.
2. At time step $n+1$ and at a specific macroiteration, $\Delta\bar{\theta}$, $\Delta\bar{\boldsymbol{\varepsilon}}$ and $\Delta\overline{\nabla\boldsymbol{\theta}}$ are provided by the **macroscale analysis**. At the beginning of the microiterations ($m^* = 0$), set at every microscopic point $\Delta\boldsymbol{\varepsilon} = \Delta\bar{\boldsymbol{\varepsilon}}$, $\Delta\nabla\boldsymbol{\theta} = \Delta\overline{\nabla\boldsymbol{\theta}}$, $\Delta\tilde{\boldsymbol{u}} = 0$, $\Delta\tilde{\theta} = 0$.
3. At every microscopic point, evaluate $\boldsymbol{\sigma}$, r, $\boldsymbol{q}$ and the microtangent thermomechanical moduli $\boldsymbol{D}^{\varepsilon}$, $\boldsymbol{D}^{\theta}$, $\boldsymbol{R}^{\varepsilon}$, R^{θ}, $\boldsymbol{\kappa}$ using the **microconstitutive law**.
4. Compute the virtual increments $\delta\tilde{\boldsymbol{u}}$ and $\delta\tilde{\theta}$ from the microequilibrium and microenergy equations
$$\text{div}\,(\boldsymbol{D}^{\varepsilon} : \text{grad}\delta\tilde{\boldsymbol{u}} + \boldsymbol{\sigma}) = 0, \qquad \text{div}\left(\boldsymbol{q} - \boldsymbol{\kappa}\cdot\text{grad}\delta\tilde{\theta}\right) = 0\,,$$
with periodic microscopic boundary conditions.
5. At every microscopic point, update the microquantities
$\Delta\tilde{\boldsymbol{u}} = \Delta\tilde{\boldsymbol{u}} + \delta\tilde{\boldsymbol{u}}$, $\delta\boldsymbol{\varepsilon} = \text{grad}_{\text{sym}}\delta\tilde{\boldsymbol{u}}$, $\Delta\boldsymbol{\varepsilon} = \Delta\boldsymbol{\varepsilon} + \delta\boldsymbol{\varepsilon}$,
$\Delta\tilde{\theta} = \Delta\tilde{\theta} + \delta\tilde{\theta}$, $\delta\nabla\boldsymbol{\theta} = \text{grad}\delta\tilde{\theta}$, $\Delta\nabla\boldsymbol{\theta} = \Delta\nabla\boldsymbol{\theta} + \delta\nabla\boldsymbol{\theta}$.
6. At every microscopic point, evaluate $\boldsymbol{\sigma}$, r, $\boldsymbol{q}$ and the microtangent thermomechanical moduli $\boldsymbol{D}^{\varepsilon}$, $\boldsymbol{D}^{\theta}$, $\boldsymbol{R}^{\varepsilon}$, R^{θ}, $\boldsymbol{\kappa}$ using the **microconstitutive law**.
7. If the convergence criterion is satisfied then continue with step 8, else return to step 4.
8. Compute the macrostress $\bar{\boldsymbol{\sigma}} = \langle\boldsymbol{\sigma}\rangle$, the macroheat flux $\bar{\boldsymbol{q}} = \langle\boldsymbol{q}\rangle$ and the macroscalar $\bar{r} = \langle r\rangle$.

Table 5 Algorithm for the microconstitutive law [58]

1. At time step n, everything is known in both scales.
2. At time step $n+1$, the time increments $\Delta\boldsymbol{\varepsilon}$ and $\Delta\nabla\boldsymbol{\theta}$ are provided by the **first part of the unit cell problem**. Moreover, $\Delta\bar{\theta}$ is known from the **macroscale analysis**.
3. The stress tensor $\boldsymbol{\sigma}$, the internal variables $\boldsymbol{\xi}$, the scalar r, and the heat flux $\boldsymbol{q}$ are computed through a **constitutive law algorithm**.
4. The thermomechanical moduli $\boldsymbol{D}^{\varepsilon}$, $\boldsymbol{D}^{\theta}$, $\boldsymbol{R}^{\varepsilon}$, R^{θ}, and $\boldsymbol{\kappa}$ are computed from a **tangent moduli algorithm**.

Internal variables are assumed to be functions of the strain and macrotemperature and the cell problem and the macroscopic problem are written via the micro- and macrotangent moduli, respectively, where the iteration increments for stress, difference between mechanical work and internal energy rate and heat flux are expressed in terms of strain, temperature, and temperature gradient increments,

$$\mathfrak{d}\boldsymbol{\sigma}^{(0)} = \boldsymbol{D}^{\varepsilon}\mathfrak{d}\boldsymbol{\varepsilon}^{(0)} + D^{\theta}\mathfrak{d}, \quad \mathfrak{d}r = \boldsymbol{R}^{\varepsilon} : \mathfrak{d}\boldsymbol{\varepsilon}^{(0)} + R^{\theta}\mathfrak{d}\bar{\theta}, \tag{5.1}$$

$$\mathfrak{d}\boldsymbol{q}^{(0)} = -\boldsymbol{k}\mathfrak{d}\nabla\boldsymbol{\theta}^{(0)}, \tag{5.2}$$

$$\mathfrak{d}\overline{\boldsymbol{\sigma}} = \overline{\boldsymbol{D}}^{\varepsilon}\mathfrak{d}\bar{\boldsymbol{\varepsilon}} + \overline{D}^{\theta}\mathfrak{d}\bar{\theta}, \quad \mathfrak{d}\bar{r} = \overline{\boldsymbol{R}}^{r} : \mathfrak{d}\bar{\boldsymbol{\varepsilon}} + \overline{R}^{\theta}\mathfrak{d}\bar{\theta}. \quad \mathfrak{d}\overline{\boldsymbol{q}} = -\boldsymbol{k}\mathfrak{d}\overline{\nabla\boldsymbol{\theta}}. \tag{5.3}$$

Table 6 Algorithm for the second part of the unit cell problem [58]

1. At every microscopic point in the unit cell the tensors $\boldsymbol{D}^{\varepsilon}$, $\boldsymbol{D}^{\theta}$, $\boldsymbol{R}^{\varepsilon}$, R^{θ} and $\boldsymbol{\kappa}$ are provided by the **first part of the unit cell problem**
2. Compute the correctors $\boldsymbol{\chi}^{\varepsilon}$, $\boldsymbol{\chi}^{\theta}$ and $\boldsymbol{\psi}^{\theta}$ from the equations
$\operatorname{div}\left(\left[\boldsymbol{D}^{\varepsilon}+\boldsymbol{D}^{\varepsilon}\tilde{:}\operatorname{grad}\boldsymbol{\chi}^{\varepsilon}\right]^{T}\right)=\boldsymbol{0}$,
$\operatorname{div}\left(\boldsymbol{D}^{\theta}+\boldsymbol{D}^{\varepsilon}:\operatorname{grad}\boldsymbol{\chi}^{\theta}\right)=\boldsymbol{0}$,
$\operatorname{div}\left(\left[\boldsymbol{\kappa}+\boldsymbol{\kappa}\tilde{:}\operatorname{grad}\boldsymbol{\psi}^{\theta}\right]^{T}\right)=\boldsymbol{0}$.
3. Evaluate the effective tangent moduli
$\overline{\boldsymbol{D}}^{\varepsilon}=\langle\boldsymbol{D}^{\varepsilon}:\boldsymbol{A}^{\varepsilon}\rangle$, $\overline{\boldsymbol{D}}^{\theta}=\langle\boldsymbol{D}^{\theta}+\boldsymbol{D}^{\varepsilon}:\boldsymbol{A}^{\theta}\rangle$, $\bar{\boldsymbol{\kappa}}=\langle\boldsymbol{\kappa}\cdot\boldsymbol{A}^{\kappa}\rangle$,
$\overline{\boldsymbol{R}}^{\varepsilon}=\langle\boldsymbol{R}^{\varepsilon}:\boldsymbol{A}^{\varepsilon}\rangle$, $\overline{\boldsymbol{R}}^{\theta}=\langle R^{\theta}+\boldsymbol{R}^{\varepsilon}:\boldsymbol{A}^{\theta}\rangle$,
where $\boldsymbol{A}^{\varepsilon}=\boldsymbol{\mathcal{I}}+\boldsymbol{\mathcal{I}}\tilde{:}\operatorname{grad}\boldsymbol{\chi}^{\varepsilon}$, $\boldsymbol{A}^{\theta}=\operatorname{grad}_{\mathrm{sym}}\boldsymbol{\chi}^{\theta}$, $\boldsymbol{A}^{\kappa}=\boldsymbol{I}+\left[\operatorname{grad}\boldsymbol{\psi}^{\theta}\right]^{T}$.

The symbol $\mathfrak{d}$ in the above expressions denotes iterational type of increment in a return mapping scheme [58]. The tangent micromoduli entering the expressions for the stress and the energy term are obtained in the unit cell problem. For specific thermodynamic potential and yield surface, analytical expressions for the microscopic moduli can be obtained by computing all variations of plastic strains, stress, local dissipation, and energy term for small variations of $\boldsymbol{\varepsilon}$, θ. Since the incremental constitutive law is linear, analytical expressions for the macroscopic moduli are obtained from the solution of the cell problem as in elasticity [10]. The cell problem is solved in two steps. In the first step, the macrostrain, macrotemperature, and macrotemperature gradient are fixed. The uncoupled equations of equilibrium and energy are solved iteratively

$$\frac{\partial}{\partial x_j}\left(\sigma_{ij}^{(0)}+D_{ijkl}^{\varepsilon}\frac{\partial\mathfrak{d}u_k^{(1)}}{\partial x_l}\right)=0,\quad \frac{\partial}{\partial x_i}\left(q_i^{(0)}-k_{ij}\frac{\partial\mathfrak{d}\theta^{(1)}}{\partial x_j}\right)=0. \tag{5.4}$$

Then, the macrostress and the macroheat flux are computed by averaging the microscopic counterparts. The final microtangent moduli are utilized in the second step.

In the second step, the macrostress, macrotemperature, and macrotemperature gradient are released. The residuals are assumed zero. By introducing the new unknown functions χ_{ijk}^{ε}, χ_i^{θ} and ψ_i^{θ}, the microincrements are written $\mathfrak{d}u_i^{(1)}=\mathfrak{d}\bar{\varepsilon}_{kl}\chi_{kli}^{\varepsilon}+\mathfrak{d}\bar{\theta}\chi_i^{\theta}$, $\mathfrak{d}\theta^{(1)}=\mathfrak{d}\overline{\nabla\boldsymbol{\theta}}_i\psi_i^{\theta}$. Then, the following uncoupled equations are solved:

$$\begin{aligned}&\frac{\partial}{\partial x_j}\left(D_{ijkl}^{\varepsilon}+D_{ijmn}^{\varepsilon}\frac{\partial\chi_{klm}^{\varepsilon}}{\partial x_n}\right)=0,\ \frac{\partial}{\partial x_j}\left(D_{ij}^{\theta}+D_{ijmn}^{\varepsilon}\frac{\partial\chi_k^{\theta}}{\partial x_l}\right)=0,\\&\frac{\partial}{\partial x_i}\left(k_{ij}^{\theta}+k_{ik}^{\varepsilon}\frac{\partial\psi_j^{\theta}}{\partial x_k}\right)=0.\end{aligned} \tag{5.5}$$

Finally, the macroscopic tangent moduli and the concentration tensors are computed:

$$\begin{aligned}&\bar{D}_{ijkl}^{\varepsilon}=\langle D_{ijmn}^{\varepsilon}A_{mnkl}\rangle,\quad \bar{D}_{ij}^{\theta}=\langle D^{\theta}+D^{\varepsilon}ij_{kl}A_{kl}^{\theta}\rangle,\quad \bar{k}_{ij}=\langle k_{ik}\Theta_{kj}\rangle,\\&\bar{R}_{ij}^{\epsilon}=\langle R_{kl}^{\varepsilon}A_{klij}^{\varepsilon}\rangle,\quad \bar{R}^{\theta}=\langle R^{\theta}+R_{ij}^{\varepsilon}A_{ij}^{\theta}\rangle,\end{aligned} \tag{5.6}$$

where

$$\begin{aligned}&A_{mnkl}=\mathfrak{I}_{mnkl}+\frac{1}{2}\left(\frac{\partial\chi_{klm}^{\varepsilon}}{\partial x_n}+\frac{\partial\chi_{kln}^{\varepsilon}}{\partial x_m}\right),\quad A_{kl}^{\theta}=\frac{1}{2}\left(\frac{\partial\chi_k^{\theta}}{\partial x_l}+\frac{\partial\chi_l^{\theta}}{\partial x_k}\right),\\&\Theta_{kj}=I_{kj}\frac{\partial\psi_j^{\theta}}{\partial x_k}.\end{aligned} \tag{5.7}$$

The above numerical scheme [50,51] follows the standard procedure; however, it is not always efficient. Alternatively, FFT-based homogenization framework has been proposed [85], following different numerical schemes, namely the Moulinec–Suquet [86], the Barzilai–Borwein [87] and the inexact Newton method [88].

6 Mean-field methodologies

In the previous Sections, periodic homogenization serves as framework for developing a multiscale strategy. In this section, other homogenization schemes are going to be examined, namely the mean-field approaches [89–91].

The most common mean-field approaches, the Mori–Tanaka [92,93] and the self-consistent [94], have been introduced for the identification of the viscoplastic response of random media [95]. Due to their numerical efficiency, mean-field and analytical methods in general have become popular for the analysis of various nonlinear mechanisms: viscoelastic [96–98], elastoplastic [99,100], viscoplastic [101], damage [102–104], damage and plasticity [105], as well as composite response under the peridynamics framework [106]. However, it is well known that the mean-field based approaches frequently produce stiff responses due to the lack of detailed information on the inelastic strains. Inelastic fields are computed only in average per phase, leading to inaccurate inelastic predictions. To address this issue, several methods have been adopted in the literature. The isotropization method has been employed for elastoplastic [107–109], viscoplastic [110], or viscoelastic–viscoplastic [111] composites. Based on the pivotal work of Ponte-Castaneda [112], many authors have proposed numerical schemes using the concept of the linear comparison composite. The related works consider the variational incremental approach [67,113–115] or the incremental-secant approach [116,117], to study the elastoplastic and the viscoplastic behavior of heterogeneous media.

The Transformation Field Analysis (TFA) [118,119] is a powerful tool for the analysis of composites undergoing nonlinear deformation. Combined with mean-field approaches, advanced models have been emerged for the analysis of composites with strongly nonlinear behavior [120,121], among them viscopasticity coupled with damage [122] and viscoelasticity [123,124]. TFA has also been combined with periodic homogenization [125]. A modified version has been introduced [126], called nonuniform Transformation Field Analysis (NTFA). The latter accounts for the nonuniformity of the plastic strain field by decomposing the anelastic strains on a set of plastic modes, which can be determined analytically or numerically [127]. The spatial variation of the modes captures the salient features of the plastic flow in the unit cell. NTFA, combined with full-field homogenization strategies, has shown excellent results for the analysis of viscoplastic [128,129] and elastoplastic [130] composites.

Recently, the Mori–Tanaka method has served as framework for studying fully coupled thermomechanical processes for composites, using the scale separation rules established from the periodic homogenization analysis. In a recent work [131], the Mori–Tanaka scheme is combined with the Transformation Field Analysis to compute mechanical and thermal fields and thermomechanical tangent moduli of a reinforced matrix, exploiting the knowledge from periodic homogenization that macrodisplacement and macrotemperature coincide with their microscopic counterparts, while their gradients are highly oscillating functions and their macroscopic counterparts must be taken equal to their average. Mori–Tanaka method is a Eshelby solution-based methodology which starts from the hypothesis that in a unit cell each inhomogeneity with its surrounding matrix is considered as an Eshelby problem. It allows for defining the so-called dilute concentration tensors for the reinforcement and then computes the total concentration tensors [58]. On the other hand, according to the TFA the total strain in each phase depends on the macrostrain and the inelastic stress at all phases. The numerical examples show the accuracy of the method under certain conditions and its capability to modelcomposites under strong interplay between mechanical and thermal loading, as well as to simulate cyclic loading under fully coupled thermomechanical conditions. This method can incorporate other inelastic mechanisms and, combined with cycle jump techniques [132,133], could be a tool on studying fatigue.

For a fiber or particulate composite with N types of reinforcement, combining the Mori–Tanaka approach and the transformation field analysis yields that the average strain fields of the reinforcements, $\boldsymbol{\varepsilon}_i$ ($i = 1, ..., N$), and of the matrix, $\boldsymbol{\varepsilon}_0$, are given by the expressions

$$\boldsymbol{\varepsilon}_i = \boldsymbol{A}_i : \bar{\boldsymbol{\varepsilon}} + \boldsymbol{A}^p_{0,i} : \boldsymbol{\sigma}^p_0 + \sum_{j=1}^{N} \boldsymbol{A}^p_{j,i} : \boldsymbol{\sigma}^p_j, \tag{6.1}$$

$$\boldsymbol{\varepsilon}_0 = \boldsymbol{A}_0 : \bar{\boldsymbol{\varepsilon}} + \boldsymbol{A}^p_0 : \boldsymbol{\sigma}^p_0 + \sum_{i=1}^{N} \boldsymbol{A}^p_{i,0} : \boldsymbol{\sigma}^p_i. \tag{6.2}$$

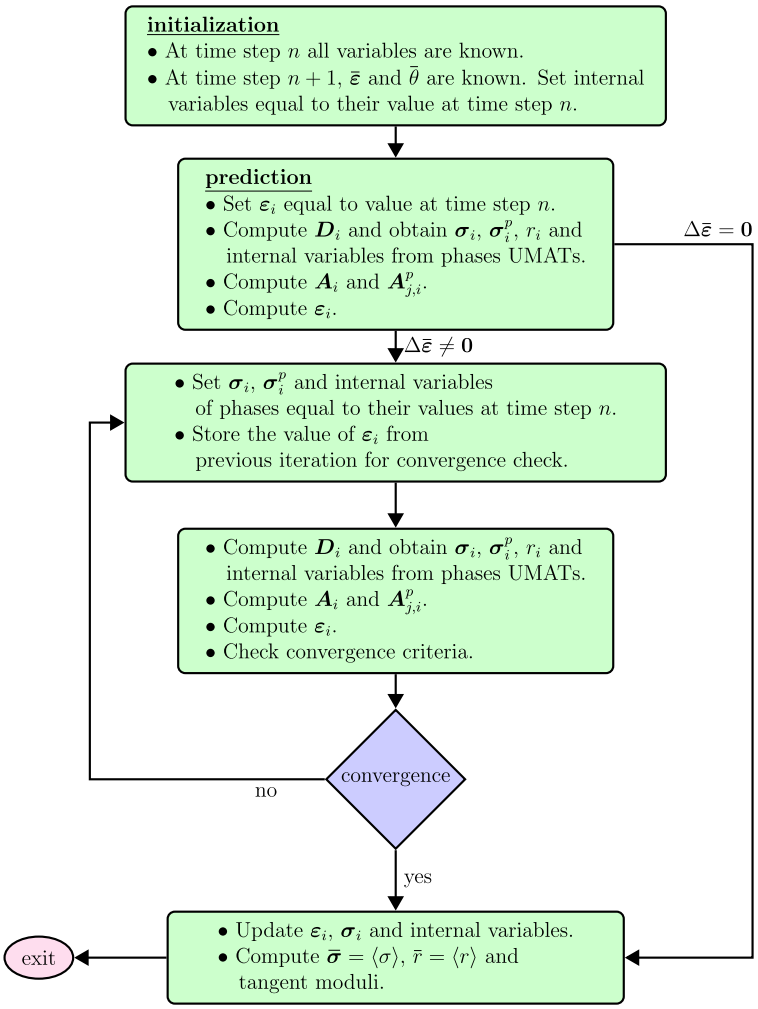

Fig. 2 Computational algorithm (Meta-UMAT) for the thermomechanical homogenization of multilayered composites. Mori–Tanaka/TFA approach. The symbol Δ denotes time increment

In the above formulas, $\boldsymbol{\sigma}_j^p$ denote the average inelastic strains in the phases, $\boldsymbol{A}_j$ are the elastic strain concentration tensors, and the $\boldsymbol{A}_{i,j}^p$ are the inelastic strain concentration tensors ($i, j = 0, 1, ..., N$). The $\boldsymbol{A}$ tensors are computed using the dilute strain concentration tensors, which are obtained from the Eshelby problem [131].

For the average temperature gradients at the phases, the classical Mori–Tanaka scheme renders the expressions

$$\boldsymbol{\nabla\theta}_i = \boldsymbol{A}_i^{\kappa} : \overline{\boldsymbol{\nabla\theta}}, \quad i = 0, 1, ..., N, \tag{6.3}$$

where $\boldsymbol{A}_i^{\kappa}$ denote the thermal concentration tensors [58].

Similar to the periodic homogenization approach, the macroscopic thermomechanical tangent moduli are computed from the expressions (5.6), using though analytical expressions for the relevant concentration tensors [134, 135], which depend on the thermomechanical tangent moduli of the phases. For structural applications, the micromechanics method can be integrated in finite element computations in a similar way with a typical constitutive law of a standard material. Figure 2 illustrates a computational algorithm for integrating the Mori–Tanaka/TFA into the FE code ABAQUS as a Meta-User Material (UMAT) subroutine. In the case of multilayered composites, the Mori–Tanaka/TFA renders the same results with the periodic homogenization (Fig. 3).

A key limitation of mean-field homogenization techniques lies in the strong assumption of uniform internal field variables within each phase. This simplification often leads to overly stiff macroscopic responses. To address this issue, several approaches have been proposed in the literature, including the isotropization of the

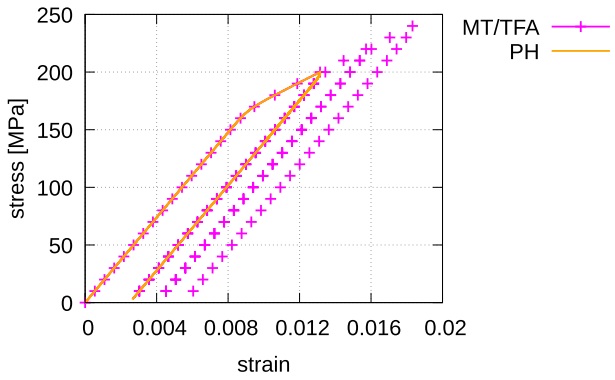

(a)

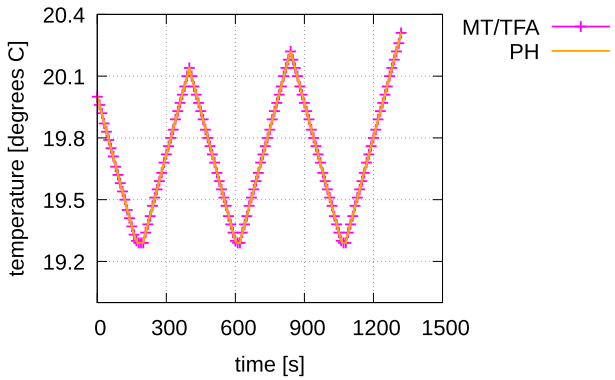

(b)

Fig. 3 Multilayered composite with 20% elastic epoxy and 80% viscoplastic steel: **a** stress–strain and **b** temperature–time curves comparison between the Mori–Tanaka/TFA (MT/TFA) scheme and the periodic homogenization (PH) [131]

tangent modulus [107], the linear comparison composite method incorporating second statistical moments [67], and the introduction of specialized interphases between the matrix and the reinforcement [120].

The computational homogenization schemes for fully coupled thermomechanical models presented so far require a considerable computational cost which is prohibitive for large scale applications. However, recent alternative methodologies like data-driven techniques and reduced order methods have been proven quite accurate and time efficient. These methods can provide robust solutions in real or near real time, while preserving the physics principles.

7 Data-driven methods and model order reduction techniques for composite materials

This section discusses briefly alternative approaches to classical homogenization schemes for the studies of composites, based on data-driven modeling and model order reduction techniques. Given the abundance of studies and recent publications on these topics, the aim is not to offer an exhaustive review but to provide the reader with a comprehensive overview of the general trends in these multiscale methods. In this regard, the section focuses on artificial neural networks (ANN) and Physics-Informed Neural Networks (PINN) for the former methods, while it discusses the Proper Orthogonal Decomposition (POD) and Proper Generalized Decomposition (PGD) techniques for the latter.

Artificial neural networks (ANNs) have recently been developed to address a variety of challenges in engineering applications, particularly in mechanics of materials and structures. These networks facilitate the replacement of traditional material laws with data-driven models informed and enriched by numerical or experimental data. Their effectiveness is further enhanced by the incorporation of constraints and conservation laws to ensure compliance with fundamental physical principles. In addition, machine learning algorithms,

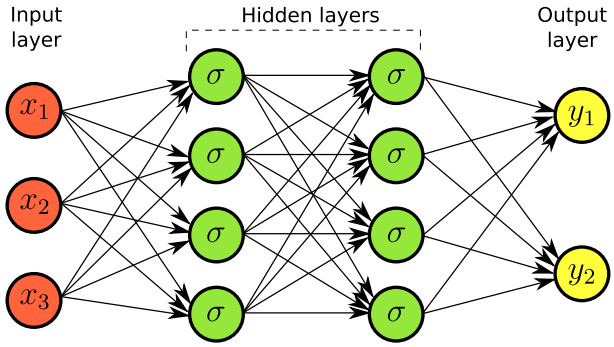

Fig. 4 Typical structure of neural network [18]

including ANNs, are increasingly used as surrogate models, providing a computationally efficient alternative for performing complex physical simulations.

A neural network is a supervised learning algorithm to a parametrized function $\boldsymbol{y} = \boldsymbol{f}_{NN}(\boldsymbol{x})$ (Fig. 4), where the $\boldsymbol{x}$ is the input data of the neural network and $\boldsymbol{f}_{NN}$ is the output, which is written as $\boldsymbol{f}_{NN}(\boldsymbol{x}) = \boldsymbol{f}_k(\boldsymbol{f}_{k-1}(...(\boldsymbol{f}_1(\boldsymbol{x}))...))$. Every function $\boldsymbol{f}_i, i = 1, 2, ..k$ corresponds to a layer after the input layer. Every neuron receives the data $\boldsymbol{x}$ or $\boldsymbol{f}_i(\boldsymbol{x})$ from the previous layer, which is transformed to the scalar $z = \boldsymbol{w}^T\boldsymbol{x} + b$, and it feeds the (nonlinear) activation function $\sigma(z(\boldsymbol{w}^T\boldsymbol{x} + b))$ for the next layer. The vector $\boldsymbol{w}$ and the scalar b are the weights and the bias, respectively.

Significant effort has been devoted in the engineering community to construct robust and accurate data-driven models for predicting the response of nonlinear materials, including elasto-plasticity [136], rate-dependent behavior [137], and thermoplastic elastomers [138]. In recent works, developed ANNs take into account physical restrictions such as the non-negative nature of dissipation [139]. In general, there is an important effort to combine data-driven models and thermodynamics in order to provide more accurate and physically informed ANNs [140]. Recently, several homogenization-enriched surrogate models have been proposed in the literature [141].

Artificial neural networks have also been implemented successfully for the modeling of composite materials [52,142]. An efficient way to introduce ANNs in heterogeneous materials modeling is by representing the macroscopic potential as a response surface parameterized by the macroscopic strains and certain microstructural parameters [143]. Micromechanics analyses have been performed using deep material networks (DMN) [144]. The latter is a data-driven technique in which the neural networks are substituted by a tree of hierarchical laminates [145]. Deep material networks have been combined with FFT homogenization to study short fiber composites under coupled thermomechanical conditions [146]. This relevant last work demonstrates a proper pathway to couple thermomechanical homogenization and artificial neural networks.

A characteristic strategy of ANN implementation in composite structures can be found in the recently proposed Multiscale Thermodynamics-Informed Neural Networks, or MuTINN [147]. This model uses two consecutive neural networks to formulate macroscopic constitutive relationships for inelastic heterogeneous materials, respecting fundamental thermomechanics-induced restrictions. The authors study a woven thermoplastic composite with 2-2 twill fabric reinforcement; however, the approach can be adopted for other types of composites too. The thermomechanical basis of the model is formed by defining: (i) the Helmholtz free energy potential for the overall composite, (ii) the macroscopic observable state variables (total strains and stresses), (iii) several "quantities of interest," resembling the internal states variables of a typical homogeneous material [148]. For both phases, the observable state variable is the macroscopic strain $\bar{\boldsymbol{\varepsilon}}$. In order to predict the time history of the inelastic behavior, without spending excessive computational cost, the "quantities of interest" $\bar{\boldsymbol{v}}$ are assumed to represent averaging of specific internal state variables for both the matrix and the reinforcement.

Figure 5 [147] illustrates the MuTINN architecture, composed from two networks: The first network corresponds to the "macroscopic-type" evolution law, while the second to the state law for the composite. The first network is fed by the macroscopic strain components $\bar{\boldsymbol{\varepsilon}}^n$ and quantities of interest $\bar{\boldsymbol{v}}^n$ at the time step n and the macroscopic strain increment $\Delta\bar{\boldsymbol{\varepsilon}}^{n+1}$. Its aim is to compute the increments $\Delta\bar{\boldsymbol{v}}^{n+1}$ and eventually the updated quantities of interest $\bar{\boldsymbol{v}}^{n+1}$. These values feed the second ANN to predict the Helmholtz free energy

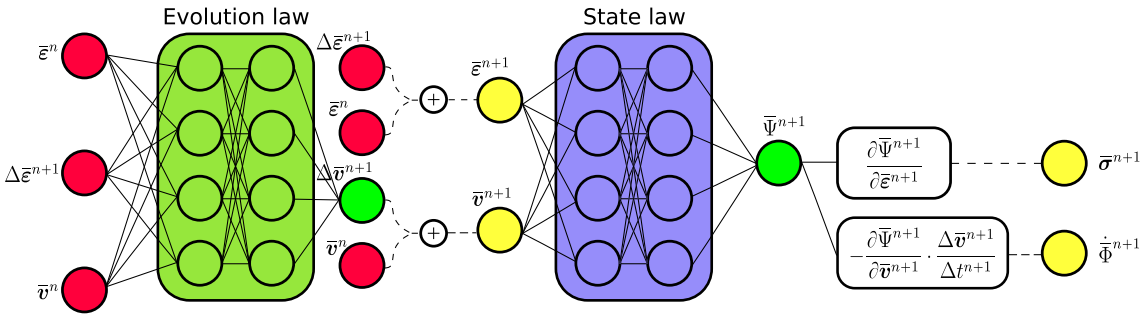

Fig. 5 Multiscale thermodynamics-informed neural networks (MuTINN) architecture. The first ANN represents the evolution law, and the second ANN describes the state law [147]

$\bar{\Psi}^{n+1}$ of the composite. Then, by an automatic differentiation procedure the macroscopic stress $\bar{\boldsymbol{\sigma}}^{n+1}$ and the dissipation

$$\dot{\bar{\Phi}} = -\frac{\partial\bar{\Psi}^{ANN}}{\partial\bar{\boldsymbol{v}}^{ANN}}\cdot\frac{\Delta\bar{\boldsymbol{v}}^{ANN}}{\Delta t},$$

at the time step $n+1$ are computed. It is noted that the dissipation is calculated for ensuring the thermodynamical consistency $\dot{\bar{\Phi}} \geq 0$ and to define the penalty term in the cost function, which is of the form

$$L = \lambda_{\bar{\boldsymbol{v}}}|\bar{\boldsymbol{v}} - \bar{\boldsymbol{v}}^{ANN}| + \lambda_{\bar{\boldsymbol{\sigma}}}|\bar{\boldsymbol{\sigma}} - \bar{\boldsymbol{\sigma}}^{ANN}| + \lambda_{\bar{\Psi}}|\bar{\Psi} - \bar{\Psi}^{ANN}| + \lambda_{\Phi}P_{\Phi}, \tag{7.1}$$

where

$$\bar{\boldsymbol{\sigma}}^{ANN} = \frac{\partial\bar{\Psi}^{ANN}}{\partial\bar{\boldsymbol{\varepsilon}}}, \tag{7.2}$$

$$P_{\Phi} = \begin{cases} 0, & \text{if } -\dfrac{\partial\bar{\Psi}^{ANN}}{\partial\bar{\boldsymbol{v}}^{ANN}}\cdot\dfrac{\Delta\bar{\boldsymbol{v}}^{ANN}}{\Delta t} \geq 0, \\ \left|-\dfrac{\partial\bar{\Psi}^{ANN}}{\partial\bar{\boldsymbol{v}}^{ANN}}\cdot\dfrac{\Delta\bar{\boldsymbol{v}}^{ANN}}{\Delta t}\right|, & \text{otherwise,} \end{cases} \tag{7.3}$$

and $\lambda_{\bar{\boldsymbol{v}}}, \lambda_{\bar{\boldsymbol{\sigma}}}, \lambda_{\bar{\Psi}}, \lambda_{\Phi}$ are the weights. It is worth noticing that the λ_{Φ} should be appropriately chosen to obtain a large value to guarantee that the second law of thermodynamics is well respected. This two-step ANN model serves as a material-type constitutive law and can be integrated into a Finite Element code (FE-MuTINN) for performing structural computations.

The MuTINN framework has shown excellent agreement with results from periodic homogenization in the case of woven composites, both in terms of mechanical fields and energies [147] (Fig. 6). In a recent study, the MuTINN has also been validated both numerically and experimentally for recycled thermoplastic composites [149] (Fig. 7).

While the above ANN type model studies the mechanical behavior of composite materials, its physics-based nature allows to address in the future thermomechanical coupling conditions. To achieve such goal, it is essential to incorporate the energy balance equation, by computing apart from the stress fields the thermomechanical coupling terms.

A special case of ANN is the so-called Physics-Informed Neural Network (PINN). Physical laws describing the problem are added, in the form of partial differential equations [18]

$$\frac{\partial\boldsymbol{u}}{\partial t} + \mathfrak{N}[\boldsymbol{u};\boldsymbol{\mu}] = 0, \tag{7.4}$$

with appropriate boundary and initial conditions, where $\mathfrak{N}[\boldsymbol{u};\boldsymbol{\mu}]$ nonlinear differential operator with coefficients $\boldsymbol{\mu}$. There are two different directions of proceeding: The first is to assume that $\boldsymbol{\mu}$ are known and to compute $\boldsymbol{u}$ for initial and boundary conditions (data-driven inference problem). The second is to assume that $\boldsymbol{u}$ is known and to identify $\boldsymbol{\mu}$. It is important to underline that the problem must be well posed and have one unique solution, in order to predict the solution by Physics-Informed Neural Network. Since networks are fully differentiable, it is possible to compute all derivatives, for both the $\boldsymbol{u}$ and the parameters $\boldsymbol{\mu}$, with respect to $\boldsymbol{x}$

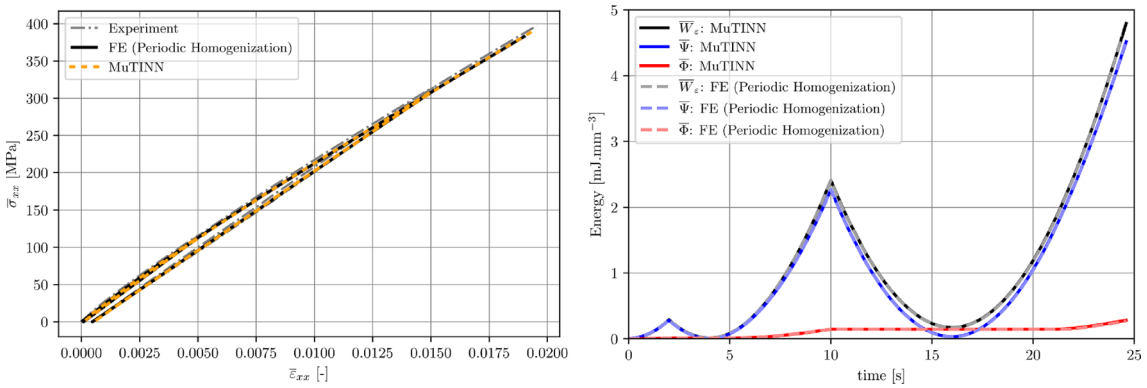

Fig. 6 Comparative analysis of load unload testing on woven composite orientations $\pm[0°]s$: experiment versus FE-based periodic homogenization versus MuTINN for stress strain curve and FE-based periodic homogenization versus MuTINN for energies [147]

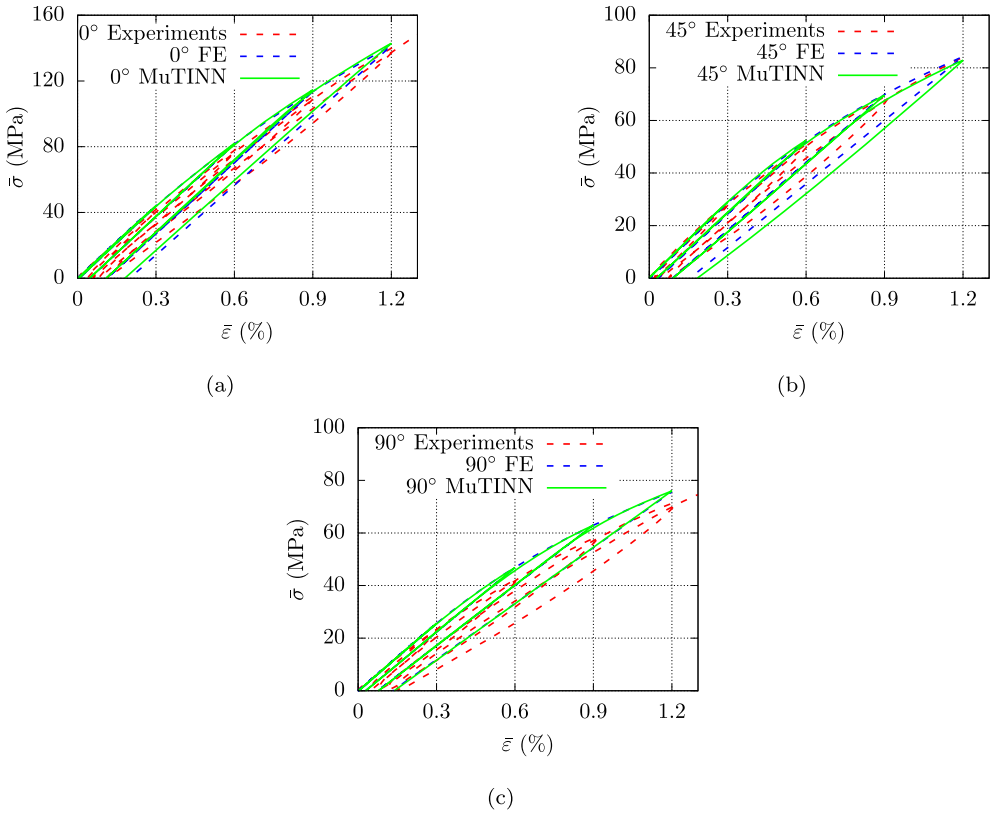

Fig. 7 Comparison of numerical and experimental results for cyclic loading and unloading at increasing strain levels for various specimen orientations in recycled thermoplastic composites [149]: **a** 0°, **b** 45°, and **c** 90°. Loading and unloading stages were controlled with a strain rate of $\dot{\varepsilon} = 8 \times 10^{-3}\ \mathrm{s}^{-1}$

and t. Then, the mean squared error loss of the partial differential equation, the boundary conditions, and the initial conditions are computed and the sum represents the cost function to be minimized.

In the recent years, the PINNs have emerged as attractive alternatives to the conventional numerical methods for solving coupled partial differential equations [150–152]. In these models, the neural network is trained on a set of collocation points to obtain the optimized weights and biases. The loss function to be minimized is composed of residuals of the governing partial differential equations and the relevant spatio-temporal boundary conditions [153]. The automatic differentiation included in the modern machine learning techniques is exploited to construct the loss function, offering an additional advantage. Physically informed deep homogenization neural network (DHN) has been developed to substitute the classical FE computations for periodic

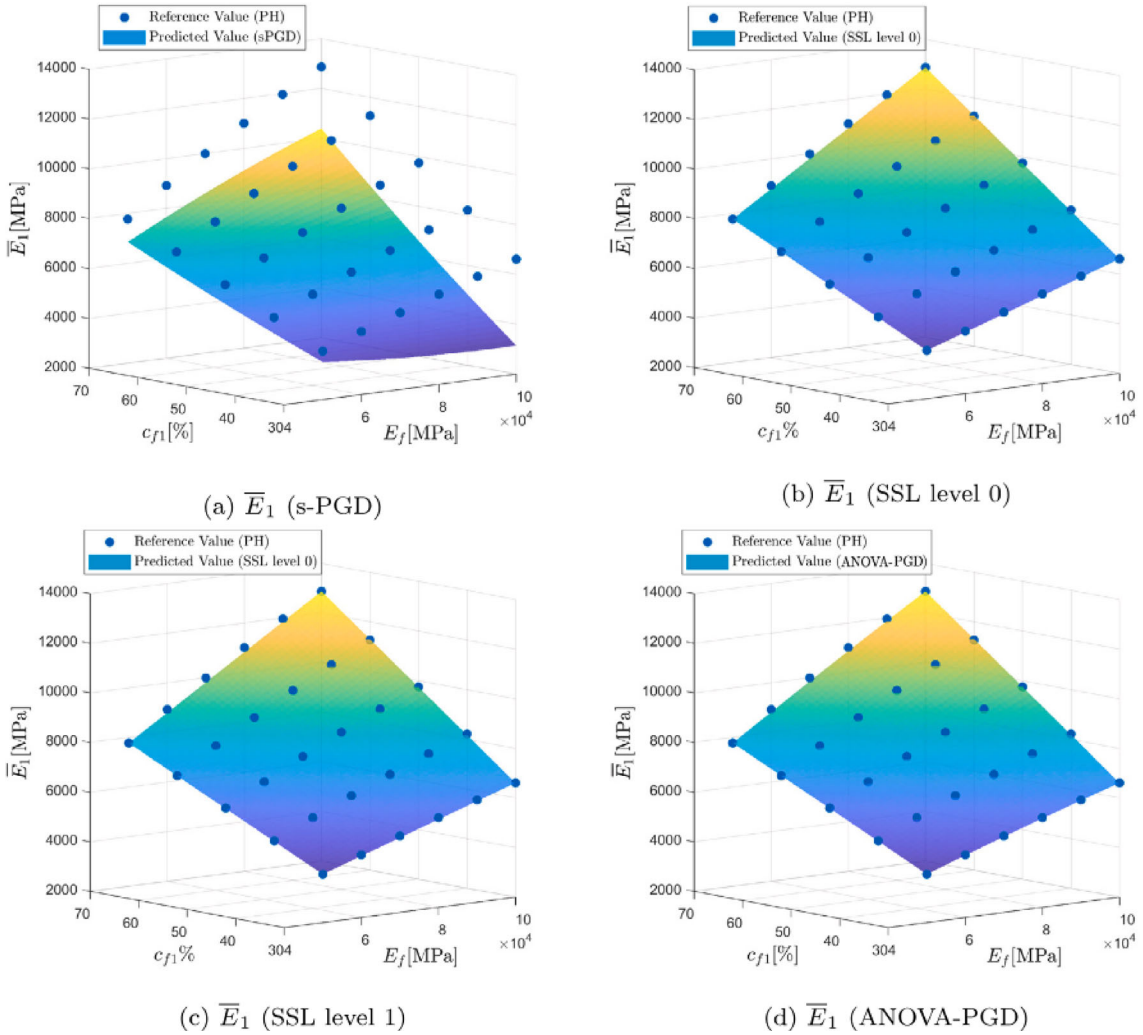

Fig. 8 Comparison between reference and predicted values of longitudinal Young modulus, as a function of fiber Young's modulus and intra-weft fiber volume fraction. **a** Values predicted by s-PGD. **b** Values predicted by SSL level 0. **c** Values predicted by SSL level 1. **d** Values predicted by ANOVA-PGD [168]

homogenization of composites. This technique resolves the system of partial differential equations using ANN with special layers accounting for the periodicity at the external surfaces of the unit cell. Such strategy has been adopted for simulating both the mechanical [154,155] and thermal responses [156] of periodic composites, while also integrating interface effects between the constituents [157], damage mechanisms [158], and large deformation processes [159]. It is also feasible to combine PINNs and higher-order multiscale theories [160].

The data-driven models, while powerful numerical tools, carry the risk of predicting non-physical responses in certain situations, especially in regimes where there is sparse or insufficient data used during their training. More physically based strategies rely on the so-called model order reduction (MOR) techniques. The Proper Orthogonal Decomposition (POD) [161] and the Proper Generalized Decomposition (PGD) [53] are characteristic examples of such strategies. The goal of MOR is to transform the real physical system into a reduced one without losing essential information. The homogenization technique of Nonlinear Transformation Field Analysis can be considered a form of MOR [126,162]. Usually order reduction techniques are applied on the differential equations (balance of linear momentum, energy balance, etc.) and can be intrusive [163–165] or non-intrusive [166–168]. The latter techniques have the advantage of not requiring a priori formulation, making them ideal for implementation in industrial applications that utilize commercial FE softwares. The main idea of the non-intrusive PGD is to approximate the solution w of the system of differential equations as

a finite sum of products of one-dimensional functions W,

$$w(p_1, ..., p_N) \approx \sum_{i=1}^{N} \prod_{j=1}^{N} W_j^i(p_j), \tag{7.5}$$

where N and M denote the number of variables and modes, respectively. Techniques such as s-PGD, Sparse Subpace Learning PGD (SSL-PGD), rs-PGD, and ANOVA-PGD [169] differ in the sampling of collocation points and the approximation features.

In a recent article [168], multiparametric solutions providing the elastic properties of woven composites have been proposed using different reduced order models, namely s-PGD, SSL levels 0 and 1, and the ANOVA-PGD. The comparisons with classical periodic homogenization (PH) reveal good agreement (Fig. 8), notably for ANOVA-PGD which requires less number of generated unit cells compared to the others. Among the first works addressing nonlinear composites, a 2010 article proposed a combination of the computational homogenization with PGD for history-dependent and history-independent materials [170]. In addition, a novel approach for hyper-reduced multiscale finite element simulations (FE^2) has been proposed in a recent relevant article [171]. The latter integrates reduction techniques commonly employed to mitigate costs like Proper Orthogonal Decomposition (POD) and hyper-reduction methods (e.g., Empirical Cubature Method, ECM), addressing the high computational costs of traditional FE^2 methods.

POD and PGD methods and their variants have been proved very efficient; however, they experience difficulties in describing strong nonlinear problems. Combining MOR and ANN has been proposed in the literature for physics-based models [172], leading to models with high accuracy and tremendous reduction in computational cost.

The main limitation of both ANN and MOR methods lies in the representativeness of the initial database. Achieving sufficient computational accuracy typically requires a large database, which significantly increases the offline computational cost. Furthermore, data-driven methods often exhibit low predictive accuracy when the input data fall outside the range of the training database.

8 Concluding remarks

This paper demonstrates that the homogenization may be used as the background for developing a multiscale strategy to investigate the fully coupled thermomechanical behavior of composites. The key points of this review can be summarized below:

- In thermomechanical processes, asymptotic expansion homogenization of zero order provides all variables and equations in both scales.
- Based on periodic homogenization findings for the fully coupled thermomechanical problem, the Helmholtz free energy, the constitutive law, and the dissipation can be approximated. In this framework, the microscale equations depend on the macroscopic temperature.
- Similar to the mechanical processes, periodic homogenization is combined with computational homogenization techniques applied to a linearized incremental scheme. Computational schemes to address the thermomechanical couplings in composites rely on performing global finite element analysis, based on Newton–Raphson iterative solution of equations of equilibrium and energy, using the concept of thermomechanical tangent moduli.
- In recent works, advanced thermomechanical homogenization numerical techniques have been developed, using FE^2 and FFT. Mean-field approaches, combined with Transformation Field Analysis, can also be adopted to capture the thermomechanical couplings.
- Higher-order homogenization theories have been successfully adopted for thermoelastic composites; however, for nonlinear responses there are still many open questions.
- Both ANNs- and PINNs-based approaches have demonstrated excellent capabilities to accurately capture the mechanical or thermal response of composites, with substantial computational time reduction. Accounting for the thermodynamic restrictions enhances the performance of the artificial neural networks and reduces the number of training data.
- Model order reduction methods based on non-intrusive PGD techniques combine numerical efficiency and adaptability on commercial software, while at the same time they are founded on the principle formulations of the classical methods in mechanics. In addition, providing multiparametric solutions, MOR can be

beneficial for composites undergoing higher-order effects (non-local phenomena), since they can provide easier numerical implementation.
- Both data-driven and MOR approaches can be modified accordingly in order to incorporate fully coupled thermomechanical effects in composites.

Acknowledgements The present work was motivated by fruitful discussions of the authors with colleagues at the Constantin Carathéodory Symposium (Celebrating 150 years from his birth) in Greece on July 10–15, 2023. Furthermore, the authors would like to warmly thank their former collaborators (PhD and Postdoc fellow), as well as their partners, who contributed to the discussions on the studies dealing with multiscale strategies of dissipative materials: Mohammed El Fallaki-Idrissi, Saif-Eddine Sekkal, Laurent Peltier, Francis Praud, Soheil Satouri, El Hadi Tikarrouchine, Qiang Chen, Adil Benaarbia, André Chrysochoos, Gilles Robert, Bjoern Kiefer, Francisco Chinesta.

Author contribution GC involved in writing the original draft, bibliographic review on the multiscale modeling , validation. NC took part in writing the original draft, bibliographic review on the mathematical homogenization, validation. FM involved in writing the review on the data-driven modeling and conclusion, bibliographic review on data-driven modeling. All authors reviewed the manuscript.

Data availability No datasets were generated or analyzed during the current study.

Declarations

Conflict of interest The authors declare no conflict of interest.

References

1. Chrysochoos, A., Huon, V., Jourdan, F., Muracciole, J.M., Peyroux, R., Wattrisse, B.: Use of full-field digital image correlation and infrared thermography measurements for the thermomechanical analysis of material behaviour. Strain **46**(1), 117–130 (2010). https://doi.org/10.1111/j.1475-1305.2009.00635.x
2. Benaarbia, A., Chatzigeorgiou, G., Kiefer, B., Meraghni, F.: A fully coupled thermo-viscoelastic-viscoplastic-damage framework to study the cyclic variability of the Taylor–Quinney coefficient for semi-crystalline polymers. Int. J. Mech. Sci. **163**, 105128 (2019). https://doi.org/10.1016/j.ijmecsci.2019.105128
3. Finazzi, D., Sinchuk, Y., Sevenois, R.D., Daelemans, L., De Clerck, K., Robert, G., Van Paepegem, W.: Study of self-heating and local strain rate in polyamide-6 and short fibre glass/polyamide-6 under tension through synchronised full-field strain and temperature measurements. Polym. Test. **132**, 108361 (2024). https://doi.org/10.1016/j.polymertesting.2024.108361
4. Benaarbia, A., Chrysochoos, A., Robert, G.: Thermomechanical behavior of PA6.6 composites subjected to low cycle fatigue. Compos. B **76**, 52–64 (2015)
5. Duvaut, G., Lions, J.-L.: Les inéquations en Mécanique et en Physique. Dunod, Paris (1972)
6. Tartar, L.: Homogénéisation et compacité par compensation, Cours Peccot, Collège de France. Partially written in Murat, F. (1977)
7. Murat, F.: H-convergence, Séminaire d'analyse fonctionnelle et numérique de l'Université d'Alger. Multicopied (1977)
8. Tartar, L.: General Theory of Homogenization. A Personalized Introduction, Lecture Notes of the Unione Matematica Italiana, 7. Springer, Milano (2008)
9. Bensoussan, A., Lions, J.-L., Papanicolaou, G.: Asymptotic Methods for Periodic Structures. North Holland (1978)
10. Sanchez-Palencia, E.: Non-homogeneous media and vibration theory. Lecture Notes in Physics 127. Springer (1978)
11. Suquet, P.M.: Elements of homogenization for inelastic solid mechanics. In: Sanchez-Palencia, E., Zaoui, A. (eds.) Homogenization Techniques for Composite Materials, pp. 193–278. Lecture Notes in Physics 272. Springer (1987)
12. Ariza, M., Conti, S., Ortiz, M.: Homogenization and continuum limit of mechanical metamaterials. Mech. Mater. **196**, 105073 (2024). https://doi.org/10.1016/j.mechmat.2024.105073
13. Johnson, C.: Existence theorems for plasticity problems. Journal de Mathematiques Pures et Appliquees **55**, 431–444 (1976)
14. Johnson, C.: On finite element methods for plasticity problems. Numer. Math. **26**, 79–84 (1976)
15. Simo, J.C., Hughes, T.J.R.: Computational Inelasticity. Springer, New York (1998). https://doi.org/10.1007/b98904
16. Ortiz, M., Simo, J.C.: An analysis of a new class of integration algorithms for elastoplastic constitutive relations. Int. J. Numer. Methods Eng. **23**, 353–366 (1986). https://doi.org/10.1002/nme.1620230303
17. Charalambakis, N., Chatzigeorgiou, G., Chemiski, Y., Meraghni, F.: Mathematical homogenization of inelastic dissipative materials: a survey and recent progress. Contin. Mech. Thermodyn. **30**, 1–51 (2018)
18. Kollmannsberger, S., D'Angella, D., Jokeit, M., Herrmann, L.: Deep Learning in Computational Mechanics. Springer, An Introductory Course (2021)
19. Aboudi, J., Pindera, M., Arnold, S.: Higher-order theory for functionally graded materials. Compos. Part B **30**, 777–832 (1999)
20. Geers, M.G.D., Kouznetsova, V.G., Brekelmans, W.A.M.: Multi-scale computational homogenization: trends and challenges. J. Comput. Appl. Math. **234**(7), 2175–2182 (2010). https://doi.org/10.1016/j.cam.2009.08.077
21. Aboudi, J.: Micromechanics-based thermoviscoplastic constitutive equations for rubber-like matrix composites at finite strains. Int. J. Solids Struct. **41**, 5611–5629 (2004)

22. Asada, T., Ohno, N.: Fully implicit formulation of elastoplastic homogenization problem for two-scale analysis. Int. J. Solids Struct. **44**, 7261–7275 (2007)
23. Cavalcante, M., Marques, S., Pindera, M.: Transient thermomechanical analysis of a layered cylinder by the parametric finite-volume theory. J. Therm. Stresses **32**, 112–134 (2009)
24. Cavalcante, M., Pindera, M.: Generalized FVDAM theory for elastic-plastic periodic materials. Int. J. Plast. **77**, 90–117 (2016)
25. Khatam, H., Pindera, M.: Parametric finite-volume micromechanics of periodic materials with elastoplastic phases. Int. J. Plast. **25**, 1386–1411 (2009)
26. Cavalcante, M., Khatam, H., Pindera, M.: Homogenization of elastic-plastic periodic materials by fvdam and fem approaches—an assessment. Compos. B **42**, 1713–1730 (2011)
27. Javili, A., Chatzigeorgiou, G., Steinmann, P.: Computational homogenization in magneto-mechanics. Int. J. Solids Struct. **50**, 4197–4216 (2013)
28. Chatzigeorgiou, G., Javili, A., Steinmann, P.: Unified magnetomechanical homogenization framework with application to magnetorheological elastomers. Math. Mech. Solids **19**(2), 194–212 (2014)
29. Bravo-Castillero, J., Rodriguez-Ramos, R., Mechkour, H., Otero, J., Cabanas, J., Sixto, L., Guinovart-Diaz, R., Sabina, F.: Homogenization and effective properties of periodic thermomagnetoelectroelastic composites. J. Mech. Mater. Struct. **4**(5), 819–836 (2009)
30. Lagoudas, D.: Shape Memory Alloys: Modeling and Engineering Applications. Springer, New York (2008)
31. Lagoudas, D., Hartl, D., Chemisky, Y., Machado, L., Popov, P.: Constitutive model for the numerical analysis of phase transformation in polycrystalline shape memory alloys. Int. J. Plast. **32–33**, 155–183 (2012)
32. Qidwai, M., Lagoudas, D.: Numerical implementation of shape memory alloy. thermomechanical constitutive model using return mapping algorithms. Int. J. Numer. Methods Eng. **40**, 1123–1168 (2002)
33. Otero, F., Oller, S., Martinez, X.: Multiscale computational homogenization: review and proposal of a new enhanced-first-order method. Arch. Comput. Methods Eng. **25**, 479–505 (2018)
34. Pierard, O., González, C., Segurado, J., LLorca, J., Doghri, I.: Micromechanics of elasto-plastic materials reinforced with ellipsoidal inclusions. Int. J. Solids Struct. **44**(21), 6945–6962 (2007). https://doi.org/10.1016/j.ijsolstr.2007.03.019
35. Wu, L., Mustafa, M., Segurado, J., Noels, L.: Second-order computational homogenisation enhanced with non-uniform body forces for non-linear cellular materials and metamaterials. Comput. Methods Appl. Mech. Eng. **407**, 115931 (2023). https://doi.org/10.1016/j.cma.2023.115931
36. Kouznetsova, V., Geers, M., Brekelmans, W.: Multi-scale second-order computational homogenization of multi-phase materials: a nested finite element solution strategy. Comput. Methods Appl. Mech. Eng. **193**(48), 5525–5550 (2004). https://doi.org/10.1016/j.cma.2003.12.073
37. Germain, P.: Cours de Mecanique des Milieux Continus. Theorie Generale, Masson, Paris, Tome I (1973)
38. Halphen, B.: Sur les discontinuites de vitesse en elastoplasticite, Comptes Rendus de l' Academie des Sciences de Paris. Ser. A-B **287**(7), A569–A572 (1978)
39. Germain, P., Nguyen, Q., Suquet, P.: Continuum thermodynamics. J. Appl. Mech. **50**, 1010–1020 (1983)
40. Hutchinson, J.: Bounds and self consistent estimates for creep of polycrystalline materials. Proc. Roy. Soc. Lond. A **348**, 101–127 (1976)
41. Sun, L., Ju, J.: Elastoplastic modeling of metal matrix composites containing randomly located and oriented spheroidal particles. J. Appl. Mech. **71**, 774–785 (2004)
42. Suquet, P.: Four exact relations for the effective relaxation function of linear viscoelastic composites. Comptes Rendus de Mecanique **340**, 387–399 (2012)
43. Sengupta, A., Papadopoulos, P., Taylor, R.: A multiscale finite element method for modeling fully coupled thermomechanical problems in solids. Int. J. Numer. Methods Eng. **91**, 1396–1405 (2012)
44. Fish, J., Shek, K., Pandheeradi, M., Shephard, M.: Computational plasticity for composite structures based on mathematical homogenization: theory and practice. Comput. Methods Appl. Mech. Eng. **148**, 53–73 (1997)
45. Herzog, H., Jacquet, E.: From a shape memory alloys model implementation to a composite behavior. Comput. Mater. Sci. **39**, 365–375 (2007)
46. Ene, H.I.: On linear thermoelasticity of composite materials. Int. J. Eng. Sci. **21**(5), 443–448 (1983)
47. Temizer, I.: On the asymptotic expansion treatement of two-scale finite thermoelasticity. Int. J. Eng. Sci. **53**, 74–84 (2012)
48. Yu, Q., Fish, J.: Multiscale asymptotic homogenization for multiphysics problems with multiple spatial and temporal scales: a coupled thermo-viscoelastic example problem. Int. J. Solids Struct. **39**, 6429–6452 (2002)
49. Bednarcyk, B.A., Aboudi, J., Arnold, S.M., Pineda, E.J.: A multiscale two-way thermomechanically coupled micromechanics analysis of the impact response of thermo-elastic-viscoplastic composites. Int. J. Solids Struct. **161**, 228–242 (2019). https://doi.org/10.1016/j.ijsolstr.2018.11.018
50. Chatzigeorgiou, G., Charalambakis, N., Chemisky, Y., Meraghni, F.: Periodic homogenization for fully coupled thermomechanical modeling of dissipative generalized standard materials. Int. J. Plast. **81**, 18–39 (2016)
51. Tikarrouchine, E., Chatzigeorgiou, G., Chemisky, Y., Meraghni, F.: Fully coupled thermo-viscoplastic analysis of composite structures by means of multi-scale three-dimensional finite element computations. Int. J. Solids Struct. **164**, 120–140 (2019)
52. Liu, X., Tian, S., Tao, F., Yu, W.: A review of artificial neural networks in the constitutive modeling of composite materials. Compos. B **224**, 109152 (2021)
53. Chinesta, F., Ladeveze, P., Cueto, E.: A short review on model order reduction based on proper generalized decomposition. Arch. Comput. Methods Eng. **18**, 395–404 (2011)
54. Remond, Y., Ahzi, S., Baniassadi, M., Garmestani, H.: Applied RVE reconstruction and homogenization of heterogeneous materials. Wiley, London (2016). https://doi.org/10.1002/9781119307563
55. Mohammed Ameen, M., Peerlings, R.H.J., Geers, M.G.D.: A quantitative assessment of the scale separation limits of classical and higher-order asymptotic homogenization. Eur. J. Mech. A Solids **71**, 89–100 (2018). https://doi.org/10.1016/j.euromechsol.2018.02.011

56. Mohammed Ameen, M.: Scale-dependent homogenization of heterogeneous microstructures: application to mechanical metamaterials. Ph.d. thesis, Technische Universiteit Eindhoven (2019)
57. Chatzigeorgiou, G., Meraghni, F., Charalambakis, N.: Multiscale Modeling Approaches for Composites. Elsevier, Amsterdam (2022). https://doi.org/10.1016/C2019-0-05214-4
58. Chatzigeorgiou, G., Charalambakis, N., Chemisky, Y., Meraghni, F.: Thermomechanical Behavior of Dissipative Composite Materials. ISTE-Elsevier (2018)
59. Tsalis, D., Baxevanis, T., Chatzigeorgiou, G., Charalambakis, N.: Homogenization of elastoplastic composites with generalized periodicity in the microstructure. Int. J. Plast. **51**, 161–187 (2013)
60. Guinovart-Sanjuan, D., Vajravelou, K., Rodriguez-Ramos, R., Guinovart-Diaz, R., Bravo-Castillero, J., Lebon, F., Sabina, F.: Analysis of effective elastic properties for shell with complex geometrical shapes. Compos. Struct. **203**, 278–285 (2018)
61. Charalambakis, N., Murat, F.: Homogenization of stratified thermoviscoplastic materials. Q. Appl. Math. **64**, 359–399 (2006)
62. Nguetseng, G.: A general convergence result for a functional related to the theory of homogenization. SIAM J. Math. Anal. **20**, 608–623 (1989)
63. Allaire, G.: Homogenization and two-scale convergence. SIAM J. Math. Anal. **23**, 1482–1518 (1992)
64. Dong, H., Zheng, X., Cui, J., Nie, Y., Yang, Z., Yang, Z.: High-order three-scale computational method for dynamic thermo-mechanical problems of composite structures with multiple spatial scales. Int. J. Solids Struct. **169**, 95–112 (2019)
65. Yang, Z., Liu, Y., Sun, Y., Jing, Y., Ma, Q.: A novel second-order reduced homogenization approach for nonlinear thermo-mechanical problems of axisymmetric structures with periodic micro-configurations. Comput. Methods Appl. Mech. Eng. **368**, 113126 (2020)
66. Ponte-Castaneda, P.: Exact second-order estimates for the effective mechanical properties of nonlinear composite materials. J. Mech. Phys. Solids **44**, 827–862 (2006)
67. Lahellec, N., Suquet, P.: On the effective behavior of nonlinear inelastic composites: I. Incremental variational principles. J. Mech. Phys. Solids **55**(9), 1932–1963 (2007)
68. Terada, K., Kikuchi, N.: A class of general algorithms for multi-scale analyses of heterogeneous media. Comput. Methods Appl. Mech. Eng. **190**, 5427–5464 (2001)
69. Praud, F., Chatzigeorgiou, G., Meraghni, F.: Fully integrated multi-scale modelling of damage and time-dependency in thermoplastic-based woven composites. Int. J. Damage Mech. **30**(2), 163–195 (2021)
70. Tikarrouchine, E., Benaarbia, A., Chatzigeorgiou, G., Meraghni, F.: Non-linear FE^2 multiscale simulation of damage, micro and macroscopic strains in polyamide 66-woven composite structures: analysis and experimental validation. Compos. Struct. **255**, 112926 (2021)
71. Nachtane, M., Meraghni, F., Chatzigeorgiou, G., Harper, L.T., Pelascini, F.: Multiscale viscoplastic modeling of recycled glass fiber-reinforced thermoplastic composites: Experimental and numerical investigations. Compos. B Eng. **242**, 110087 (2022). https://doi.org/10.1016/j.compositesb.2022.110087
72. Chatzigeorgiou, G., Chemisky, Y., Meraghni, F.: Computational micro to macro transitions for shape memory alloy composites using periodic homogenization. Smart Mater. Struct. **24**(3), 035009 (2015). https://doi.org/10.1088/0964-1726/24/3/035009
73. Dondeti, P., Paquet, D., Ghosh, S.: A rate-dependent homogenization based continuum plasticity-damage (HCPD) model for dendritic cast aluminum alloys. Eng. Fract. Mech. **89**, 75–97 (2012)
74. Michel, J., Moulinec, H., Suquet, P.: Effective properties of composite materials with periodic microstructure: a computational approach. Comput. Methods Appl. Mech. Eng. **172**, 109–143 (1999)
75. Schneider, M.: An FFT-based fast gradient method for elastic and inelastic unit cell homogenization problems. Comput. Methods Appl. Mech. Eng. **315**, 846–866 (2017)
76. Schneider, M.: A review of nonlinear FFT-based computational homogenization methods. Rev. Perspect. Mech. **232**, 2051–2100 (2021)
77. Onimus, F., Gelebart, L., Brenner, R.: Polycrystalline simulations of in-reactor deformation of recrystallized Zircaloy-4 tubes: Fast Fourier Transform computations and mean-field self-consistent model. Int. J. Plast. **153**, 103272 (2022)
78. Haj-Ali, R., Aboudi, J.: Formulation of the high-fidelity generalized method of cells with arbitrary cell geometry for refined micromechanics and damage in composites. Int. J. Solids Struct. **47**(25–26), 3447–3461 (2010)
79. Chen, Q., Wang, G., Chen, X., Geng, J.: Finite-volume homogenization of elastic/viscoelastic periodic materials. Compos. Struct. **182**, 457–470 (2017)
80. Chen, Q., Pindera, M.J.: Homogenization and localization of elastic-plastic nanoporous materials with Gurtin-Murdoch interfaces: An assessment of computational approaches. Int. J. Plast **124**, 42–70 (2020)
81. Tu, W., Pindera, M.J.: Damage evolution in cross-ply laminates revisited via cohesive zone model and finite-volume homogenization. Compos. B **86**, 40–60 (2016)
82. Du, X., Chen, Q., Chatzigeorgiou, G., Meraghni, F., Zhao, G., Chen, X.: Nitsche's method enhanced isogeometric homogenization of unidirectional composites with cylindrically orthotropic carbon/graphite fibers. Compos. Sci. Technol. **256**, 110787 (2024). https://doi.org/10.1016/j.compscitech.2024.110787
83. Hanoun, I., Chatzigeorgiou, G., Meraghni, F.: Hierarchical micromechanical modeling for CNT-coated fuzzy fiber composites accounting for viscoplasticity and interfacial damage. Int. J. Solids Struct. **318**, 113409 (2025). https://doi.org/10.1016/j.ijsolstr.2025.113409
84. Berthelsen, R., Denzer, R., Oppermann, P., Menzel, A.: Computational homogenisation for thermoviscoplasticity: application to thermally sprayed coatings. Comput. Mech. **60**(5), 739–766 (2017)
85. Wicht, D., Schneider, M., Böhlke, T.: Computing the effective response of heterogeneous materials with thermomechanically coupled constituents by an implicit fast Fourier transform-based approach. Int. J. Numer. Meth. Eng. **122**, 1307–1332 (2021)
86. Moulinec, H., Suquet, P.: A numerical method for computing the overall response of nonlinear composites with complex microstructure. Comput. Methods Appl. Mech. Eng. **157**(1–2), 69–94 (1998). https://doi.org/10.1016/S0045-7825(97)00218-1

87. Schneider, M.: On the Barzilai-Borwein basic scheme in FFT-based computational homogenization. Int. J. Numer. Meth. Eng. **118**(8), 482–494 (2019). https://doi.org/10.1002/nme.6023
88. Kabel, M., Böhlke, T., Schneider, M.: Efficient fixed point and Newton–Krylov solvers for FFT-based homogenization of elasticity at large deformations. Comput. Mech. **54**(6), 1497–1514 (2014)
89. Eshelby, J.D.: The determination of the elastic field of an ellipsoidal inclusion, and related problems. Proc. R. Soc. Lond. A **241**(1226), 376–396 (1957). https://doi.org/10.1098/rspa.1957.0133
90. Christensen, R.M.: Mechanics of Composite Materials. Dover, London (1979)
91. Mura, T.: Micromechanics of Defects in Solids, Second, Revised Edition. Kluwer Academic Publishers, Dordrecht (1987). https://doi.org/10.1007/978-94-009-3489-4
92. Mori, T., Tanaka, K.: Average stress in matrix and average elastic energy of materials with misfitting inclusions. Acta Metal. **21**, 571–574 (1973)
93. Benveniste, Y.: A new approach to the application of Mori-Tanaka's theory in composite materials. Mech. Mater. **6**, 147–157 (1987). https://doi.org/10.1016/0167-6636(87)90005-6
94. Hill, R.: A self consistent mechanics of composite materials. J. Mech. Phys. Solids **13**(4), 213–222 (1965). https://doi.org/10.1016/0022-5096(65)90010-4
95. Mercier, S., Molinari, A.: Homogenization of elastic-viscoplastic heterogeneous materials: self-consistent and Mori-Tanaka schemes. Int. J. Plast. **25**, 1024–1048 (2009)
96. Vu, Q.H., Brenner, R., Castelnau, O., Moulinec, H., Suquet, P.: A self-consistent estimate for linear viscoelastic polycrystals with internal variables inferred from the collocation method. Modell. Simul. Mater. Sci. Eng. **20**(17), 024003 (2012)
97. Brenner, R., Suquet, P.: Overall response of viscoelastic composites and polycrystals: exact asymptotic relations and approximate estimates. Int. J. Solids Struct. **50**(10), 1824–1838 (2013)
98. Schöneich, M., Dinzart, F., Sabar, H., Berbenni, S., Stommel, M.: A coated inclusion-based homogenization scheme for viscoelastic composites with interphases. Mech. Mater. **105**, 89–98 (2017)
99. Zecevic, M., Knezevic, M.: Latent hardening within the elasto-plastic self-consistent polycrystal homogenization to enable the prediction of anisotropy of AA6022-T4 sheets. Int. J. Plast. **105**, 141–163 (2018)
100. Kotha, S., Ozturk, D., Ghosh, S.: Parametrically homogenized constitutive models (PHCMs) from micromechanical crystal plasticity FE simulations, part I: Sensitivity analysis and parameter identification for Titanium alloys. Int. J. Plast **120**, 296–319 (2019)
101. Rao, W., Zhang, J., Kang, G., Yu, C., Jiang, H.: A meso-mechanical constitutive model of bulk metallic glass composites considering the local failure of matrix. Int. J. Plast **115**, 238–267 (2019)
102. Desrumaux, F., Meraghni, F., Benzeggagh, M.L.: Generalised Mori–Tanaka scheme to model anisotropic damage using numerical Eshelby tensor. J. Compos. Mater. **35**(7), 603–624 (2001)
103. Meraghni, F., Desrumaux, F., Benzeggagh, M.L.: Implementation of a constitutive micromechanical model for damage analysis in glass mat reinforced composite structures. Compos. Sci. Technol. **62**(16), 2087–2097 (2002)
104. Jendli, Z., Meraghni, F., Fitoussi, J., Baptist, D.: Multi-scales modelling of dynamic behaviour for discontinuous fibre SMC composites. Compos. Sci. Technol. **69**(1), 97–103 (2009)
105. Yun, G.J., Zhu, F.-Y., Lim, H.J., Choi, H.: A damage plasticity constitutive model for wavy CNT nanocomposites by incremental Mori-Tanaka approach. Compos. Struct. **258**, 113178 (2021)
106. Buryachenko, V.A.: Generalized Mori–Tanaka approach in peridynamic micromechanics of multilayered composites of random structure. J. Peridyn. Nonlocal Model. **6**, 602–625 (2024)
107. Doghri, I., Ouaar, A.: Homogenization of two-phase elasto-plastic composite materials and structures: study of tangent operators, cyclic plasticity and numerical algorithms. Int. J. Solids Struct. **40**(7), 1681–1712 (2003)
108. Chaboche, J., Kanoute, P., Ross, A.: On the capabilities of mean-field approaches for the description of plasticity in metal matrix composites. Int. J. Plast. **21**, 1409–1434 (2005)
109. Jiang, T., Shao, J.-F.: On the incremental approach for nonlinear homogenization of composite and influence of isotropization. Comput. Mater. Sci. **46**, 447–451 (2009)
110. Czarnota, C., Kowalczyk-Gajewska, K., Salahouelhadj, A., Martiny, M., Mercier, S.: Modeling of the cyclic behavior of elastic-viscoplastic composites by the additive tangent Mori–Tanaka approach and validation by finite element calculations. Int. J. Solids Struct. **56–57**, 96–117 (2015)
111. Miled, B., Doghri, I., Brassart, L., Delannay, L.: Micromechanical modeling of coupled viscoelastic-viscoplastic composites based on an incrementally affine formulation. Int. J. Solids Struct. **50**(10), 1755–1769 (2013)
112. Ponte-Castaneda, P.: The effective mechanical properties of nonlinear isotropic composites. J. Mech. Phys. Solids **39**, 45–71 (1991)
113. Lahellec, N., Suquet, P.: Effective response and field statistics in elasto-plastic and elasto-viscoplastic composites under radial and non-radial loadings. Int. J. Plast **42**, 1–30 (2013)
114. Brassart, L., Stainier, L., Doghri, I., Delannay, L.: Homogenization of elasto-(visco) plastic composites based on an incremental variational principle. Int. J. Plast. **36**, 86–112 (2012)
115. Boudet, J., Auslender, F., Bornert, M., Lapusta, Y.: An incremental variational formulation for the prediction of the effective work-hardening behavior and field statistics of elasto-(visco)plastic composites. Int. J. Solids Struct. **83**, 90–113 (2016)
116. Wu, L., Noels, L., Adam, L., Doghri, I.: An implicit-gradient-enhanced incremental-secant mean-field homogenization scheme for elasto-plastic composites with damage. Int. J. Solids Struct. **50**(24), 3843–3860 (2013)
117. Wu, L., Adam, L., Doghri, I., Noels, L.: An incremental-secant mean-field homogenization method with second statistical moments for elasto-visco-plastic composite materials. Mech. Mater. **114**, 180–200 (2017)
118. Dvorak, G.: Transformation field analysis of inelastic composite materials. Proc. Roy. Soc. Lond. A **437**, 311–327 (1992)
119. Dvorak, G., Benveniste, Y.: On transformation strains and uniform fields in multiphase elastic media. Proc. Roy. Soc. Lond. A **437**, 291–310 (1992)
120. Barral, M., Chatzigeorgiou, G., Meraghni, F., Leon, R.: Homogenization using modified mori tanaka and tfa framework for elastoplastic-viscoelastic-viscoplastic composites: theory and numerical validation. Int. J. Plast. **127**, 102632 (2020)

121. Chatzigeorgiou, G.: Study of multilayered composites through periodic homogenization and Mori-Tanaka methods. Mech. Mater. **164**, 104110 (2022)
122. Kruch, S., Chaboche, J.L.: Multi-scale analysis in elasto-viscoplasticity coupled with damage. Int. J. Plast. **27**, 2026–2039 (2011)
123. Chen, Q., Chatzigeorgiou, G., Meraghni, F.: Extended mean-field homogenization of viscoelastic-viscoplastic polymer composites undergoing hybrid progressive degradation induced by interface debonding and matrix ductile damage. Int. J. Solids Struct. **210–211**, 1–17 (2021). https://doi.org/10.1016/j.ijsolstr.2020.11.017
124. Chen, Q., Chatzigeorgiou, G., Robert, G., Meraghni, F.: Viscoelastic-viscoplastic homogenization of short glass-fiber reinforced polyamide composites (PA66/GF) with progressive interphase and matrix damage: new developments and experimental validation. Mech. Mater. **164**, 104081 (2022)
125. Alaimo, G., Auricchio, F., Marfia, S., Sacco, E.: Optimization clustering technique for PieceWise Uniform Transformation Field Analysis homogenization of viscoplastic composites. Comput. Mech. **64**, 1495–1516 (2019)
126. Michel, J.C., Suquet, P.: Nonuniform transformation field analysis. Int. J. Solids Struct. **40**(25), 6937–6955 (2003)
127. Michel, J.C., Suquet, P.: Computational analysis of nonlinear composite structures using the nonuniform transformation field analysis. Comput. Methods Appl. Mech. Eng. **193**, 5477–5502 (2004). https://doi.org/10.1016/j.cma.2003.12.071
128. Roussette, S., Michel, J.C., Suquet, P.: Nonuniform transformation field analysis of elastic-viscoplastic composites. Compos. Sci. Technol. **69**, 22–27 (2009). https://doi.org/10.1016/j.compscitech.2007.10.032
129. Covezzi, S., de Miranda, F., Marfia, S., Sacco, E.: Complementary formulation of the TFA for the elasto-plastic analysis of composites. Compos. Struct. **156**, 93–100 (2016)
130. Ju, X., Mahnken, R., Xu, Y., Liang, L.: NTFA-enabled goal-oriented adaptive space-time finite elements for micro-heterogeneous elastoplasticity problems. Comput. Methods Appl. Mech. Eng. **398**, 115199 (2022)
131. Chatzigeorgiou, G., Meraghni, F., Chen, Q.: Fully coupled nonlinear thermomechanical modeling of composites using mean-field mori tanaka scheme combined with tfa theory. Int. J. Solids Struct. **296**, 112828 (2024)
132. Cojocaru, D., Karlsson, A.M.: A simple numerical method of cycle jumps for cyclically loaded structures. Int. J. Fatigue **28**(12), 1677–1689 (2006)
133. Chen, Q., Chatzigeorgiou, G., Robert, G., Meraghni, F.: Combination of mean field micromechanics and cycle jump technique for cyclic response of PA66/GF composites with viscoelastic-viscoplastic and damage mechanisms. Acta Mech. **234**, 1533–1552 (2023)
134. Hatta, H., Taya, M.: Equivalent inclusion method for steady state heat conduction in composites. Int. J. Eng. Sci. **24**(7), 1159–1172 (1986). https://doi.org/10.1016/0020-7225(86)90011-X
135. Benveniste, Y., Dvorak, G.J., Chen, T.: On diagonal and elastic symmetry of the approximate effective stiffness tensor oh heterogeneous media. J. Mech. Phys. Solids **39**(7), 927–946 (1991). https://doi.org/10.1016/0022-5096(91)90012-D
136. Eghbalian, M., Pouragha, M., Wan, R.: A physics-informed deep neural network for surrogate modeling in classical elasto-plasticity. Comput. Geotech. **159**, 105472 (2023)
137. Jung, S., Ghaboussi, J.: Neural network constitutive model for rate-dependent materials. Comput. Struct. **84**(15–16), 955–963 (2006)
138. Rodríguez-Sánchez, A.E., Ledesma-Orozco, E., Ledesma, S., Vidal-Lesso, A.: Application of artificial neural networks to map the mechanical response of a thermoplastic elastomer. Mater. Res. Express **6**, 075320 (2019)
139. Danoun, A., Prulière, E., Chemisky, Y.: Thermodynamically consistent Recurrent Neural Networks to predict non linear behaviors of dissipative materials subjected to non-proportional loading paths. Mech. Mater. **173**, 104436 (2022)
140. Cueto, E., Chinesta, F.: Thermodynamics of learning physical phenomena. Arch. Computat. Methods Eng. **30**, 4653–4666 (2023)
141. Wang, Y., Soutis, C., Ando, D., Sutou, Y., Narita, F.: Application of deep neural network learning in composites design. Eur. J. Mater. **2**(1), 118–171 (2022)
142. Zhang, Z., Friedrich, K.: Artificial neural networks applied to polymer composites: a review. Compos. Sci. Technol. **63**, 2029–2044 (2003)
143. Le, B.A., Yvonnet, J., He, Q.-C.: Computational homogenization of nonlinear elastic materials using neural networks. Int. J. Numer. Methods Eng. **104**(12), 1061–1084 (2015)
144. Liu, Z., Wu, C.T., Koishi, M.: A Deep Material Network for Multiscale Topology Learning and Accelerated Nonlinear Modeling of Heterogeneous Materials. Comput. Methods Appl. Mech. Eng. **345**, 1138–1168 (2019)
145. Gajek, S., Schneider, M., Bölke, T.: On the micromechanics of deep material networks. J. Mech. Phys. Solids **142**, 103984 (2020)
146. Gajek, S., Schneider, M., Böhlke, T.: An FE-DMN method for the multiscale analysis of thermomechanical composites. Comput. Mech. **69**, 1087–1113 (2022)
147. El Fallaki Idrissi, M., Praud, F., Meraghni, F., Chinesta, F., Chatzigeorgiou, G.: Multiscale thermodynamics-informed neural networks (MuTINN) towards fast and frugal inelastic computation of woven composite structures. J. Mech. Phys. Solids **184**, 105604 (2024)
148. Masi, F., Stefanou, I.: Multiscale modeling of inelastic materials with Thermodynamics-based artificial neural networks (TANN). Comput. Methods Appl. Mech. Eng. **398**, 115190 (2022)
149. Sekkal, S.E., El Fallaki Idrissi, M., Meraghni, F., Chatzigeorgiou, G., Chinesta, F.: Multiscale thermodynamics-informed neural networks (MuTINN) for nonlinear structural computations of recycled thermoplastic composites. Compos. Part B **300**, 112455 (2025). https://doi.org/10.1016/j.compositesb.2025.112455
150. Samaniego, E., Anitescu, C., Goswami, S., Nguyen-Thanh, V., Guo, H., Hamdia, K., Zhuang, X., Rabczuk, T.: An energy approach to the solution of partial differential equations in computational mechanics via machine learning: concepts, implementation and applications. Comput. Methods Appl. Mech. Eng. **362**, 112790 (2020)
151. Haghighat, E., Raissi, M., Moure, A., Gomez, H., Juanes, R.: A physics-informed deep learning framework for inversion and surrogate modeling in solid mechanics. Comput. Methods Appl. Mech. Eng. **379**, 113741 (2021)
152. Vahab, M., Haghighat, E., Khaleghi, M., Khalili, N.: A physics-informed neural network approach to solution and identification of biharmonic equations of elasticity. J. Eng. Mech. **148**, 04021154 (2022)

153. Raissi, M., Perdikaris, P., Karniadakis, G.: Physics-informed neural networks: a deep learning framework for solving forward and inverse problems involving nonlinear partial differential equations. J. Comput. Phys. **378**, 687–707 (2019)
154. Wu, J., Jiang, J., Chen, Q., Chatzigeorgiou, G., Meraghni, F.: Deep homogenization networks for elastic heterogeneous materials with two- and -three dimensional periodicity. Int. J. Solids Struct. **284**, 112521 (2023)
155. Wu, J., Chen, Q., Jiang, J., Chatzigeorgiou, G., Meraghni, F.: Adaptive deep homogenization theory for periodic heterogeneous materials. Compos. Struct. **340**, 118171 (2024)
156. Jiang, J., Wu, J., Chen, Q., Chatzigeorgiou, G., Meraghni, F.: Physically informed deep homogenization neural network for unidirectional multiphase/multi-inclusion thermoconductive composites. Comput. Methods Appl. Mech. Eng. **409**, 115972 (2023)
157. Chen, Q., Chatzigeorgiou, G., Meraghni, F., Chen, X., Yang, Z.: Physics-informed deep homogenization approach for random nanoporous composites with energetic interfaces. Eng. Appl. Artif. Intell. **140**, 109735 (2025). https://doi.org/10.1016/j.engappai.2024.109735
158. Chen, Q., Tu, W., Wu, J., He, Z., Chatzigeorgiou, G., Meraghni, F., Yang, Z., Chen, X.: Elasticity-inspired data-driven micromechanics theory for unidirectional composites with interfacial damage. Eur. J. Mech. A Solids **111**, 105506 (2025). https://doi.org/10.1016/j.euromechsol.2024.105506
159. Chen, Q., Du, X., Chatzigeorgiou, G., Meraghni, F., Zhao, G., Yang, Z.: Physics-informed deep neural networks towards finite strain homogenization of unidirectional soft composites. Eur. J. Mech. A Solids **114**, 105752 (2025). https://doi.org/10.1016/j.euromechsol.2025.105752
160. Linghu, J., Gao, W., Dong, H., Nie, Y.: Higher-order multi-scale physics-informed neural network (HOMS-PINN) method and its convergence analysis for solving elastic problems of authentic composite materials. J. Comput. Appl. Math. **456**, 116223 (2025)
161. Lu, K., Jin, Y., Chen, Y., Yang, Y., Hou, L., Zhang, Z., Li, Z., Fu, C.: Review for order reduction based on proper orthogonal decomposition and outlooks of applications in mechanical systems. Mech. Syst. Signal Process. **123**, 264–297 (2019)
162. Fritzen, F., Böhlke, T.: Reduced basis homogenization of viscoelastic composites. Compos. Sci. Technol. **76**, 84–91 (2013)
163. Ammar, A., Huerta, A., Chinesta, F., Cueto, E., Leygue, A.: Parametric solutions involving geometry: a step towards efficient shape optimization. Comput. Methods Appl. Mech. Eng. **268**, 178–193 (2014)
164. Courard, A., Néron, D., Ladevèze, P., Ballere, L.: Integration of PGD-virtual charts into an engineering design process. Compos. Sci. Technol. **63**, 2029–2044 (2016)
165. Lu, Y., Blal, N., Gravouil, A.: Multi-parametric space-time computational vademecum for parametric studies: application to real time welding simulations. Finite Elem. Anal. Des. **139**, 62–72 (2018)
166. Zou, X., Conti, M., Díez, P., Auricchio, F.: A nonintrusive proper generalized decomposition scheme with application in biomechanics. Int. J. Numer. Methods Eng. **113**, 230–251 (2018)
167. Germoso, C., Quaranta, G., Duval, J.L., Chinesta, F.: Non-intrusive in-plane-out-of-plane separated representation in 3D parametric elastodynamics. Computation **8**(3), 78 (2020)
168. El Fallaki Idrissi, M., Praud, F., Champaney, V., Chinesta, F., Meraghni, F.: Multiparametric modelling of composite materials based on non-intrusive PGD informed by multiscale analyses: application for real-time stiffness prediction of woven composites. Compos. Struct. **302**, 116228 (2022)
169. Sancarlos, A., Champaney, V., Duval, J.-L., Cueto, E., Chinesta, F.: PGD-based advanced nonlinear multiparametric regressions for constructing metamodels at the scarce-data limit (2021). arXiv:2103.05358
170. Lamari, H., Ammar, A., Cartraud, P., Legrain, G., Chinesta, F., Jacquemin, F.: Routes for efficient computational homogenization of nonlinear materials using the proper generalized decompositions. Arch. Comput. Methods Eng. **17**, 373–391 (2010). https://doi.org/10.1016/j.mechmat.2025.105444
171. Lange, N., Hütter, G., Kiefer, B.: Empirical hyper element integration method (EHEIM) with unified integration criteria for efficient hyper-reduced FE^2 simulations. Mech. Mater. **210**, 105444 (2025). https://doi.org/10.1016/j.mechmat.2025.105444
172. Barnett, J., Farhat, C., Maday, Y.: Neural-network-augmented projection-based model order reduction for mitigating the Kolmogorov barrier to reducibility. J. Comput. Phys. **492**, 112420 (2023)